Point mutations in the PDX1 transactivation domain impair human β-cell development and function

Xianming Wang [1,2,3], Michael Sterr [1,2,3], Ansarullah [1,2], Ingo Burtscher [1,2], Anika Böttcher [1,2], Julia Beckenbauer [1,2], Johanna Siehler [1,2,3], Thomas Meitinger [4], Hans-Ulrich Häring [5,6,8], Harald Staiger [5,7,8], Filippo M. Cernilogar [9], Gunnar Schotta [9], Martin Irmler [10], Johannes Beckers [8,10,11], Christopher V.E. Wright [12,13], Mostafa Bakhti [1,2,8], Heiko Lickert [1,2,3,8,*]

ABSTRACT

Objective: Hundreds of missense mutations in the coding region of *PDX1* exist; however, if these mutations predispose to diabetes mellitus is unknown.

Methods: In this study, we screened a large cohort of subjects with increased risk for diabetes and identified two subjects with impaired glucose tolerance carrying common, heterozygous, missense mutations in the *PDX1* coding region leading to single amino acid exchanges (P33T, C18R) in its transactivation domain. We generated iPSCs from patients with heterozygous $PDX1^{P33T/+}$, $PDX1^{C18R/+}$ mutations and engineered isogenic cell lines carrying homozygous $PDX1^{P33T/P33T}$, $PDX1^{C18R/C18R}$ mutations and a heterozygous *PDX1* loss-of-function mutation ($PDX1^{+/-}$).

Results: Using an *in vitro* β-cell differentiation protocol, we demonstrated that both, heterozygous $PDX1^{P33T/+}$, $PDX1^{C18R/+}$ and homozygous $PDX1^{P33T/P33T}$, $PDX1^{C18R/C18R}$ mutations impair β-cell differentiation and function. Furthermore, $PDX1^{+/-}$ and $PDX1^{P33T/P33T}$ mutations reduced differentiation efficiency of pancreatic progenitors (PPs), due to downregulation of PDX1-bound genes, including transcription factors *MNX1* and *PDX1* as well as insulin resistance gene *CES1*. Additionally, both $PDX1^{P33T/+}$ and $PDX1^{P33T/P33T}$ mutations in PPs reduced the expression of PDX1-bound genes including the long-noncoding RNA, *MEG3* and the imprinted gene *NNAT*, both involved in insulin synthesis and secretion.

Conclusions: Our results reveal mechanistic details of how common coding mutations in *PDX1* impair human pancreatic endocrine lineage formation and β-cell function and contribute to the predisposition for diabetes.

1. INTRODUCTION

Diabetes mellitus is a group of heterogeneous disorders characterized by high blood glucose levels that are caused by the loss and/or dysfunction of the pancreatic insulin-producing β-cells. The mechanisms leading to the onset of this multifactorial disease still need to be identified, and advancements will aid in improved diagnostics and personalized therapy [1]. The major forms of diabetes include type 1 (T1D) and type 2 diabetes (T2D), gestational diabetes, and maturity-onset diabetes of the young (MODY) [2]. Among these, MODYs are clinically heterogeneous monogenic forms with autosomal-dominant inheritance that result from loss-of-function mutations in key genes involved in β-cell development or function [3]. In humans 13 different MODYs have been characterized so far including MODY4, which is associated with haploinsufficiency of the transcription factor (TF) pancreas/duodenum homeobox protein 1 (PDX1) [4,5], one of the master regulators of pancreas development and β-cell function. The *PDX1* gene encodes a TF containing a transactivation domain and DNA binding homeodomain. In mouse, Pdx1 not only is important for induction and growth of the embryonic pancreas but also plays a

[1]Institute of Diabetes and Regeneration Research, Helmholtz Zentrum München, 85764 Neuherberg, Germany [2]Institute of Stem Cell Research, Helmholtz Zentrum München, 85764 Neuherberg, Germany [3]Technische Universität München, Ismaningerstraße 22, 81675 München, Germany [4]Institute of Human Genetics, Helmholtz Zentrum München, Neuherberg, Germany [5]Institute for Diabetes Research and Metabolic Diseases of the Helmholtz Zentrum München at the University of Tübingen, 72076 Tübingen, Germany [6]Department of Internal Medicine, Division of Endocrinology, Diabetology, Vascular Medicine, Nephrology and Clinical Chemistry, University of Tübingen, 72076 Tübingen, Germany [7]Institute of Pharmaceutical Sciences, Department of Pharmacy and Biochemistry, Eberhard Karls University Tübingen, 72076 Tübingen, Germany [8]German Center for Diabetes Research (DZD), 85764 Neuherberg, Germany [9]Biomedical Center and Center for Integrated Protein Science Munich, Ludwig-Maximilians-University, 82152 Planegg-Martinsried, Germany [10]Institute of Experimental Genetics, Helmholtz Zentrum München, 85764 Neuherberg, Germany [11]Chair of Experimental Genetics, School of Life Sciences Weihenstephan, Technische Universität München, 85354 Freising, Germany [12]Vanderbilt University Program in Developmental Biology, Department of Cell and Developmental Biology, Vanderbilt University, Nashville, TN 37232, USA [13]Vanderbilt Center for Stem Cell Biology, Vanderbilt University, Nashville, TN 37232, USA

*Corresponding author. Helmholtz Zentrum München, Ingolstaedter Landstraße 1, 85764 Neuherberg, Germany. Fax: +49 89 31873761. E-mail: heiko.lickert@helmholtz-muenchen.de (H. Lickert).

crucial role during insulin-producing β- and somatostatin-producing δ-cell development and function in the adult organ [6–9]. Homozygous Pdx1-deficient mice fail to generate a pancreas [10], while heterozygous animals develop a pancreas but become diabetic in adulthood due to β-cell apoptosis [11–13]. In humans, several missense coding mutations in *PDX1* gene such as the P33T and C18R mutations in the transactivation domain have been associated with and increased risk for diabetes of the carrier individuals [14–16]. Currently, there are more than 150 missense coding mutations described for *PDX1* among which mutations at amino acid position 18 and 33 are rather common (gnomad.broadinstitute.org); however, causal link to increased risk for type 2 diabetes is still missing for most mutations [17]. In contrast, *PDX1*[P33T/+] and *PDX1*[C18R/+] mutations have been shown to perturb the activity of the PDX1 protein and reduce the expression of insulin gene in INS-1 and NES2Y cell lines [15,16] although the exact mechanisms by which these mutations contribute to diabetes predisposition are not understood. Moreover, whether these mutations exert their effects through impairment in developmental programs, regulating β-cell differentiation or adult β-cell function remains unclear. Although several studies have shed light on the developmental impacts of other coding mutations of pancreatic TFs such as *PDX1*, *HNF1B*, *GATA4*, and *GATA6* [18–20], how common mutations in the *PDX1* gene affect human pancreatic progenitors and β-cells still needs to be addressed. The major obstacle is a lack of appropriate modeling systems to investigate the effect of loss-of-function or point mutations in certain genes on human pancreas development. One of the appealing approaches is the generation of induced pluripotent stem cells (iPSCs) from somatic cells from diabetic patients [21,22]. In such a system, patient-derived somatic cells are reprogrammed to generate patient-specific stem cells, which can be further differentiated into the endocrine lineage cells, mimicking human β-cell development in a culture dish [19,23,24]. Alternatively, advancements in CRISPR-Cas9 gene-editing technology offer targeting of specific mutations in the genes of interest to generate disease-specific cells and investigate the corresponding consequences [20,25].

Previously, we identified the genome-wide target gene profile of PDX1 in human pancreatic progenitors [26]. However, how PDX1 coordinates human pancreatic cell development is not understood in detail. To address this, we investigated the impact of *PDX1* coding mutations as well as its haploinsufficiency (*PDX1*^{+/−}) on differentiation of human pancreatic cells from progenitor stage to β-cells. First, we screened a large cohort of human subjects with high risk to develop diabetes and identified individuals with insulin secretion deficiency associated with heterozygous *PDX1*[P33T/+] and *PDX1*[C18R/+] missense mutations. Using patient-derived iPSCs, we found that both heterozygous mutations impair *in vitro* β-cell differentiation and function. To further exclude genetic background variations in the human population and investigate dose-dependent effects, we generated isogenic iPSC lines carrying homozygous *PDX1*[P33T/P33T] and *PDX1*[C18R/C18R] point mutations. Our results indicate that homozygous point mutations in the PDX1 transactivation domain do not only impact pancreatic endocrine lineage development, but also impair glucose-responsive function of β-cells through misregulation of several PDX1 target genes involved in β-cell development, maturation, and function. Altogether, our data provide novel insight into the mechanisms by which common point mutations in the PDX1 transactivation domain impair human pancreatic β-cell formation and function and contribute to increased risk for diabetes in the general population.

2. MATERIALS AND METHODS

2.1. Ethics statement
The choice of appropriate human donors, the procedures for skin biopsy, isolation of dermal fibroblasts, generation of iPSCs, and their use in further scientific investigations were performed under the positive vote of the Ethics Committee of the Medical Faculty of the Eberhard Karls University, Tübingen. The study design followed the principles of the Declaration of Helsinki. All study participants gave informed consent prior to entry into the study.

2.2. Cell culture
hiPSCs were cultured on 1:100 diluted Matrigel (BD Biosciences, CA, Cat #354277) in mTeSR™1 medium (STEMCELL technologies, Cat #85850). At ∼70−80% confluency, cultures were rinsed with 1 × DPBS without Mg^{2+} and Ca^{2+} (Invitrogen, Cat #14190) followed by incubation with TrypLE Select Enzyme (1 ×) (Life Technologies, Cat #12563011) for 3−5 min at 37 °C. Single cells were rinsed with mTeSR™1 medium, and spun at 1,000 rpm for 3 min. The resulting cell pellet was resuspended in mTeSR™1 medium supplemented with Y-27632 (10 μM; Sigma−Aldrich; MO, Cat #Y0503), and the single cell suspension was seeded at ∼0.75 × 10^5 cells/cm^2 on Matrigel-coated surfaces. Cultures were fed every day with mTeSR™1 medium and differentiation was initiated 72 h following seeding with ∼90% starting confluency. All the cell lines were confirmed mycoplasma-free by using the Lonza MycoAlert Mycoplasma Detection Kit (Lonza, Cat #LT07-418).

2.3. 1st pancreatic lineage differentiation protocol

2.3.1. S1: definitive endoderm (3 d)
Cells were first rinsed with 1 × DPBS without Mg^{2+} and Ca^{2+} and then exposed to MCDB 131 medium (Life Technologies, Cat #10372-019) further supplemented with 1.5 g/l sodium bicarbonate (Sigma, MO, Cat #S6297), 1 × Glutamax (Life Technologies, Cat #35050-079), 10 mM final glucose (Sigma, Cat #G8769) concentration, 0.5% bovine serum albumin fraction V, fatty acid free (Sigma, Cat # 10775835001), 100 ng/ml Activin-A (R&D Systems Inc, Cat #338-AC-050/CF), and 3 μM or 5 μM of CHIR-99021 (GSK3β inhibitor, SelleckChem, Cat #S2924) for day 1. For day 2, cells were cultured in MCDB 131 medium with 0.5% BSA, 1.5 g/l sodium bicarbonate, 1 × Glutamax, 10 mM glucose, 100 ng/ml Activin-A and 0.3 μM CHIR-99021. On day 3, cells were cultured in MCDB 131 with 0.5% BSA, 1.5 g/l sodium bicarbonate, 1 × Glutamax, 10 mM glucose and 100 ng/ml Activin-A.

2.3.2. S2: primitive gut tube (2 d)
Cells were rinsed with 1 × DPBS without Mg^{2+} and Ca^{2+} and then exposed to MCDB 131 medium further supplemented with 1.5 g/l sodium bicarbonate, 1 × Glutamax, 10 mM final glucose concentration, 0.5% BSA, 0.25 mM ascorbic acid (Sigma, Cat #A4544), 50 ng/ml FGF7 (R & D Systems, Cat #251-KG-010/CF) or/and 1.25 μM IWP-2 (Tocris Bioscience, Cat #3533) for 2 d.

2.3.3. S3: posterior foregut (2 d)
Cells were then added for 2 d in MCDB 131 medium supplemented with 2.5 g/l sodium bicarbonate, 1 × Glutamax, 10 mM glucose concentration, 2% BSA, 0.25 mM ascorbic acid, 50 ng/ml FGF7, 0.25 μM SANT-1 (Sigma, Cat #S4572), 1 μM retinoic acid (RA; Sigma, Cat #R2625), 100 nM LDN193189 (LDN; BMP receptor inhibitor, Stemgent, CA, Cat #04-0019), 1:200 ITS-X (Life Technologies, Cat

#51500056), and 200 nM TPB (PKC activator, custom synthesis, ChemPartner).

2.3.4. S4: pancreatic endoderm (3 d)
Cells were exposed to MCDB 131 medium supplemented with 2.5 g/l sodium bicarbonate, 1 × Glutamax, 10 mM final glucose concentration, 2% BSA, 0.25 mM ascorbic acid, 2 ng/ml of FGF7, 0.25 μM SANT-1, 0.1 μM retinoic acid, 200 nM LDN193189, 1:200 ITS-X, and 100 nM TPB for 3 d.

After 3 d of culture, the S4 cells were treated for 4 h with 10 μM Y-27632. Cells were then rinsed with 1 × DPBS without Mg^{2+} and Ca^{2+} and exposed to TrypLE Select Enzyme (1 ×) (Life Technologies, Cat #12563011) for 3−5 min at 37 °C. The released cells were washed with basal MCDB 131 medium and spun at 1,000 rpm for 3 min. Cell pellets were resuspended in S5-7 media with S5 chemical supplements at ∼50 million cells/ml and spotted onto Transwell insert filters (6-well plate: Corning 3414) for culture in air-liquid interface at 10 μl/spot and ∼10 spots per well. S5-7 media with supplements were added to the bottom of each insert: ∼1.5 ml per well.

2.3.5. S5: pancreatic endocrine precursors (3 d)
Cells were further cultured in MCDB 131 medium supplemented with 1.5 g/l sodium bicarbonate, 1 × Glutamax, 20 mM glucose, 2% BSA, 0.25 μM SANT-1, 0.05 μM retinoic acid, 100 nM LDN193189, 1:200 ITS-X, 1 μM T3 (3,3′,5-Triiodo-ʟ-thyronine sodium salt, Sigma, T6397), 10 μM ALK5 inhibitor ll (Enzo Life Sciences, NY, Cat #ALX-270-445), 10 μM zinc sulfate (Sigma, Z0251) and 10 μg/ml of heparin (Sigma, H3149).

2.3.6. S6: immature β-like cells (7 d)
Cells were exposed to the MCDB 131 medium further supplemented with 1.5 g/l sodium bicarbonate, 1 × Glutamax, 20 mM glucose, 2% BSA, 100 nM LDN193189, 1:200 ITS-X, 1 μM T3, 10 μM ALK5 inhibitor ll, 10 μM zinc sulfate, 100 nM gamma secretase inhibitor XX (EMD MilliPore, MA, Cat #565789) and 10 μg/ml of heparin for 7 d.

2.3.7. S7: mature β-like cells (14 d)
Cells were further cultured in MCDB 131 medium supplemented with 1.5 g/l sodium bicarbonate, 1 × Glutamax, 20 mM final glucose concentration, 2% BSA, 1:200 ITS-X, 1 μM T3, 10 μM ALK5 inhibitor ll, 10 μM zinc sulfate, 1 mM N-acetyl cysteine (N-Cys, Sigma, Cat #A9165), 10 μM Trolox (Vitamin E analogue, EMD, Cat #648471), 2 μM R428 (AXL inhibitor, SelleckChem, Cat #S2841) and 10 μg/ml of heparin for 14 d. For all stages, the cultures were fed every day.

2.4. 2nd generation pancreatic progenitor differentiation protocol

2.4.1. S1: definitive endoderm (3 d)
iPSCs plated on 1:100 diluted Matrigel were first rinsed with 1 × DPBS without Mg^{2+} and Ca^{2+} (Invitrogen) and then cultured in RPMI 1640 medium (Invitrogen, Cat #21875-034) further supplemented with 1.2 g/L sodium bicarbonate (Sigma), 0.2% ESC-qualified FBS (Life Technologies, Cat #16141-079), 100 ng/mL Activin-A (R&D Systems), and 20 ng/mL of Wnt3A (R&D Systems, Cat #5036-WN-010) for day 1 only. For the next 2 days, cells were cultured in RPMI with 0.5% FBS, 1.2 g/L sodium bicarbonate and 100 ng/mL Activin-A.

2.4.2. S2: primitive gut tube (3 d)
Cells were rinsed with 1 × DPBS (without Mg^{2+} and Ca^{2+}) once and then exposed to DMEM-F12 (Life Technologies, Cat #21041025) medium further supplemented with 2 g/L sodium bicarbonate, 2% FBS and 50 ng/mL of FGF7 for 3 days.

2.4.3. S3: posterior foregut (4 d)
Cultures were maintained for 4 days in DMEM-HG medium (Life Technologies, Cat #41966029) supplemented with 0.25 μM SANT-1 (Sigma−Aldrich), 2 μM retinoic acid (RA; Sigma−Aldrich), 100 ng/mL of Noggin (R&D Systems, Cat #6057-NG-025), and 1% B27 (Invitrogen, Cat #17504044).

2.5. Generation of clonal hiPSC mutant lines using gRNA or gRNA/ssDNA transfection in hiPSCs
All mutant lines were generated using a previously established protocol [27]. The plasmid for transfection (pU6-(BbsI) sgRNA_CAG-venus-bpA, Addgene ID86985) was a gift from from Dr. Ralf Kühn and contained BbsI site for single or multiple gRNAs, the *Venus* gene and the *Cas9* gene. Human iPSCs were cultured for two days and then dissociated using TrypLE select, replated onto Matrigel-coated plates and transfected in suspension with gRNAs or gRNA/ssDNA using Lipofectamine RNAiMAX (Thermo Fisher Scientific, Cat #13778-150) following manufacturer's instructions. For one well of 6-well plates, $0.75 × 10^6$ cells were seeded. For the $PDX1^{+/-}$ knockout cell line, 2.5 ug plasmid of gRNA was added for one transfection. For the point mutations, 2.5 ug plasmid with the gRNA and 30 pmol ssDNA were added in one transfection. gRNAs or gRNA/ssDNA and Lipofectamine RNAiMAX were diluted separately in Opti-MEM (Thermo Fisher Scientific, Cat # 31985070), mixed together, incubated for 5 min at room temperature (R.T.), and added dropwise to the hiPSCs before plating.

2.6. Establishment of clonal hiPSC mutant lines
Two days after the gRNA or gRNA/ssDNA transfection, hiPSCs were dissociated into single cells and the transfected positive cells characterized by Venus expression were sorted by FACS. After that, the sorted cells were replated at a low density (500-1,000 cells per 10 cm dish). The remaining cells were collected and genomic DNA was extracted. T7 endonuclease I assay was then performed to assess the CRISPR mutagenesis efficiency. The seeded cells were allowed to grow and form colonies from single cells. Medium was changed every 2 days. 10 days later, individual colonies were picked, mechanically disaggregated and replated in mTeSR™1 medium into individual wells of 96-well plates coated with Matrigel. Clonal lines were expanded. A portion of the cells was lysed to gain genomic DNA. Then PCR was performed using Herculase II Fusion DNA Polymerase (Agilent Technologies, Cat #600679) followed by Sanger sequencing to identify mutant clones. Primers for *PDX1* are as follows: forward: *TACCTGGGCCTAGCCTCTTAGTG*, reverse: *TGAGAACCGGAAAGGA-GAAAGGG*. Clonal cell lines carrying desired mutations were further expanded and frozen down.

2.7. Immunofluorescence imaging
Cells were fixed with 4% paraformaldehyde for 30 min and then permeabilized in PBS containing 0.2% Triton X-100. Cells were blocked with PBS containing 3% BSA, and incubated with primary antibodies overnight at 4 °C. Then the cells were incubated with the secondary antibodies for 1 h at room temperature after washing with PBS. Images were acquired on a TCS SP5 laser-scanning microscope (Leica). The following antibodies and dilutions were used: goat anti-OCT-3/4 (1:500, Cat #sc-8628, Santa Cruz), goat anti-SOX2 (1:500, Cat #sc-17320, Santa Cruz), mouse anti-TRA-1-81 (1:50, Cat #MAB4381, Millipore), mouse anti-SSEA4 (1:500, Cat #4755, Cell Signaling), rabbit anti-FOXA2 (1:250, Cat #8186, Cell Signaling), goat anti-SOX17 (1:500, Cat #GT15094, Acris/Novus), goat anti-PDX1 (1:500, Cat #AF2419, R&D Systems), rabbit anti-NKX6.1 (1:300, Cat

#NBP1-82553, Acris/Novus), guinea pig anti-C-Peptide (1:100, Cat #ab30477, Abcam), mouse anti-Glucagon (1:500, Cat #G2654, Sigma), rat anti-Somatostatin (1:300, Cat #MA5-16987, Invitrogen).

2.8. Flow cytometry

Cells were dissociated using $1 \times$ TrypLE Select Enzyme and collected. After that, cells were washed with cold FACS buffer (5% FBS in $1 \times$ DPBS). Cells were fixed with 4% paraformaldehyde and permeabilized with donkey block solution (0.1% tween-20, 10% FBS, 0.1% BSA and 3% donkey serum) containing 0.5% saponin. The cells were incubated with rabbit anti-FOXA2 (1:200, #8186, Cell Signaling), goat anti-SOX17 antibody (1:200, Cat #GT15094, Acris/Novus), goat anti-PDX1 antibody (1:100, Cat #AF2419, R&D Systems), rabbit anti-NKX6.1 antibody (1:200, Cat #NBP1-82553, Acris/Novus), guinea pig anti-C-Peptide antibody (1:100, Cat #ab30477, Abcam), mouse anti-Glucagon (1:500, Cat #G2654, Sigma), for 30 min at room temperature and then stained with appropriate AlexaFluor-555 and -647 secondary antibody for 30 min at room temperature. Flow cytometry was performed using FACS-Aria III (BD Bioscience). FACS data were analyzed using FlowJo. For quantification of median fluorescence intensity (MFI) for PDX1, the PDX1 positive population was first gated and then MFI was calculated using BD FACS software.

2.9. RNA isolation and qPCR

Total RNA was extracted from cells with the miRNeasy mini kit (Qiagen). cDNA synthesis was performed with a high-capacity RNA-to-cDNA kit (Applied Biosystems). TaqMan qPCR was performed under standard conditions using ViiA7 (Applied Biosystems) and TaqMan Fast Advanced Master Mix (Applied Biosystems). Samples were normalized to the housekeeping genes 18S ribosomal RNA (*RNA18S*) and glyceraldehyde 3-phosphate dehydrogenase (*GAPDH*). Taqman probes (Applied Biosystems): *INS*, Hs02741908_m1; *GCG*, Hs01031536_m1; *SST*, Hs00356144_m1; *PDX1*, Hs00236830_m1; *GAPDH*, Hs02758991_g1; *18S*, Hs99999901_s1; *NKX6.1*, Hs01055914_m1; *MAFA*, Hs01651425_s1; *NEUROD1*, Hs01922995_s1; *UCN3*, Hs00846499_s1; *PAX6*, Hs01088114_m1; *ABCC8*, Hs01093752_m1; *KCNJ11*, Hs00265026_s1; *SLC30A8*, Hs00545183_m1.

2.10. Affymetrix microarray

For microarray analysis, total RNA from $PDX1^{P33T/+}$ and XM001 PPs, produced with the 2nd differentiation protocol, was extracted using the miRNeasy Mini kit (Qiagen, Cat #217004). RNA integrity was checked using the Agilent 2100 Bioanalyzer (Agilent RNA 6000 Pico Kit) and cDNA was amplified with the Ovation PicoSL WTA System V2 (Nugen, 3312) in combination with the Encore Biotin Module (Nugen, USA). Amplified cDNA was hybridized on GeneChip™ Human Gene 2.0 ST arrays (Affymetrix, 902113). Expression console (v.1.3.0.187, Affymetrix) was used for quality control. All subsequent computational analysis was performed in R using Bioconductor packages. Expression data were RMA normalized using the oligo package (version 1.38.0) and probe sets were annotated using the package hugene20sttranscriptcluster.db (version 8.5.0). Differential expression analyses were performed on prefiltered data, containing the 30562 probe sets with highest expression values, using the limma package (version 3.30.7) and p-values were adjusted for multiple testing by Benjamini-Hochberg correction. A gene was considered differentially expressed if the adjusted p-value (FDR) was below a threshold of 0.1 and the fold-change was greater than or equal to 2. Functional enrichments were conducted using HOMER [28]. Functional annotations were based on term affiliations provided by HOMER and literature research.

2.11. ChIP-seq

All samples for ChIP-seq were processed as described in [26]. $PDX1^{P33T/+}$ PP cells (2×10^6 cells) were cross-linked in 1% formaldehyde in culture medium for 10 min at room temperature. The cross-linking reaction was stopped by the addition of glycine to a final concentration of 125 mM. For chromatin fragmentation, cells were resuspended in lysis buffer (50 mM Tris-HCl (pH 8.0), 10 mM EDTA, 0.5% SDS) and sonicated in a Covaris S220 sonicator with a duty cycle of 2%, a peak incident power of 105 W and 200 cycles per burst for 20 min. The fragmented chromatin was diluted 1:5 in IP-Buffer (10 mM Tris-HCl (pH 7.5), 1 mM EDTA, 0.5 mM EGTA, 1% Triton X-100, 0.1% SDS, 0.1% Na-Desoxycholate, 140 mM NaCl, H_2O, Protease Inhibitors) and directly used for immunoprecipitation. For PDX1 ChIP, 60% of the chromatin (equivalent of 1.2×10^6 cells) was processed in two parallel ChIPs using magnetic beads, preloaded with 3 µl goat anti PDX1 antibody (kindly provided by C. Wright), for each ChIP. For H3K27ac ChIP, 40% of the chromatin (equivalent 0.4×10^6 cells) was processed in three parallel IPs using magnetic beads, preloaded with 3 µg anti H3K27ac antibody (Diagenode, C15410174). For all ChIPs, antibody incubation was performed at 4 °C for 5 h. Beads were then washed 5 times using (1.) IP-Buffer, (2.) Washing-Buffer 1 (500 mM NaCl, 50 mM Tris-HCl (pH 8.0), 0.1% SDS, 1% NP-40), (3.) Washing-Buffer 2 (250 mM LiCl, 50 mM Tris-HCl (pH 8.0), 0.5% Na-Deoxycholate, 1% NP-40) and (4. & 5.) Washing-Buffer 3 (10 mM Tris-HCl (pH 8.0), 10 mM EDTA). Subsequently, protein-DNA complexes were eluted from the beads in Elution-Buffer (50 mM Tris-HCl (pH 8.0), 10 mM EDTA, 1% SDS) at 65 °C for 20 min. Cross-links were reversed at 65 °C overnight and DNA was purified for library construction using the MicroPlex kit (Diagenode, C05010010).

2.12. ChIP-seq data analysis

For all processing and analysis steps, $PDX1^{P33T/+}$ data from this study was used together with data from XM001 cells, previously published by our group (GSE106950) [26]. Raw reads from PDX1 and H3K27ac ChIP-seq were processed with Trimmomatic (0.35) to remove low quality bases and potential adapter contamination. Next, reads were aligned to hg19 genome using bowtie2 (2.2.6) with very-sensitive option and duplicate reads were removed using samtools (1.3). BAM files from $PDX1^{P33T/+}$ cells were subsampled to match the read depth of the BAM files from XM001 cells using samtools. Binding sites of PDX1 in XM001 and $PDX1^{P33T/+}$ cells were then called using GEM (3.2) in multi condition mode and filtered, after visual inspection, using a Q-value cut-off of 10^{-4} (XM001) and $10^{-4.05}$ ($PDX1^{P33T/+}$). Subsequently, overlapping regions were merged. Regions of H3K27ac enrichment were called using HOMER (4.10) on the merged data from XM001 and $PDX1^{P33T/+}$ cells using parameters -style histone -size 500 -minDist 2000. PDX1 binding sites and H3K27ac enriched regions were further filtered by removing blacklist regions. H3K27ac read counts from XM001 and $PDX1^{P33T/+}$ cells were normalized using a set of promoters from housekeeping genes [29]. Housekeeping genes were derived from the microarray data and defined by an absolute log2 fold change ($PDX1^{P33T/+}$ vs XM001) < log2 (1.1) and a linear coefficient of variation < 0.15. Reads were counted in a region from 1000 bp upstream to 100 bp downstream of the TSS of the housekeeping genes and DESeq2 (1.20) was used to estimate size factors for normalization. Normalized read counts where used when indicated in the figures. Regions and binding sites within 20 kb of a TSS or within a gene body were annotated with the respective gene using bedtools (2.26.0). Motif analysis, annotations with genomic features and pathway enrichment analysis were performed using HOMER. To calculate enrichment of H3K27ac at PDX1-bound sites, three sets of

random sites were generated by shuffling all PDX1 binding sites from $PDX1^{P33T/+}$ cells using bedtools (2.26.0) shuffle. Then, H3K27ac reads were counted and ratio of the mean read count at PDX1 sites over the mean read count at shuffled sites was calculated. For visualization, BIGWIG files were generated from downsampled BAM files and normalized using the size factors previously determined by DESeq2 (H3K27ac only) using deeptools bamCoverage (3.1.0).

2.13. RNA-seq

RNA samples from $PDX1^{+/-}$, $PDX1^{P33T/P33T}$, $PDX1^{C18R/C18R}$ and XM001 lines were collected at the PP1 stage were produced by the 1st differentiation protocol. Total RNA from $PDX1^{+/-}$, $PDX1^{P33T/P33T}$, $PDX1^{C18R/C18R}$, and XM001 lines was extracted using miRNeasy Mini kit (Qiagen, #217004) and RNA integrity was checked using Agilent 2100 Bioanalyzer (Agilent RNA 6000 Pico Kit). Libraries were prepared using the TruSeq Stranded mRNA Library Prep (Illumina).

2.14. RNA-seq analysis

RNA-seq data was quantified using salmon (0.11.3) quant with options — validateMappings — rangeFactorizationBins 4 — numBootstraps 100 — seqBias — gcBias. Quantification results were imported into R using tximport. DESeq2 (1.20) [30] was used for differential expression analysis as follows. Genes with less than 6 reads were discarded and DESEq2 was run with default parameters. Results were calculated with independent filtering and independent hypothesis weighting [31]. For the comparison PPs against iPSCs, all data sets were used and all PP samples (i.e. XM001, $PDX1^{C18R/C18R}$, $PDX1^{P33T/P33T}$, and $PDX1^{+/-}$) were compared with XM001 iPSCs using the lfcThreshold = 1.5 option in the results function. For the comparison of the different PP cells, only data from PPs were loaded into DESeq2. Results for these comparisons were generated without the lfcThreshold option. For all analyses, fold changes were shrunken using the apeglm method [32] using the results from independent hypothesis weighting. Genes were considered as differentially expressed when the FDR was >0.05 (PP vs iPSC) or 0.1 (PDX1 mutations vs control) and absolute shrunken log2 fold change was >2 (PP vs iPSC) or 1 (PDX1 mutations vs control). GO-term and pathway analysis were performed using HOMER.

2.15. Static glucose stimulation insulin secretion

Static glucose stimulated insulin secretion (GSIS) of the generated β-like cells was performed based on previous protocols [18,20]. Briefly, 5 aggregates were picked and rinsed three times with KRBH buffer (129 mM NaCl, 4.8 mM KCl, 2.5 mM CaCl2, 1.2 mM MgSO4, 1 mM Na2HPO4, 1.2 mM KH2PO4, 5 mM NaHCO3, 10 mM HEPES and 0.1% BSA in deionized water and sterile filtered) and then equilibrated in KRBH buffer at 37 °C for 1 h. Aggregates then were incubated in KRBH buffer with 2.8 mM glucose for 60 min at R.T. Supernatants were collected, and the aggregates were transferred to KRBH buffer with 16.7 mM glucose for 60 min. Supernatants were collected again. At the end of the experiment, cell aggregates were dissociated into single cells and the cell numbers were counted to normalize the GSIS. Mercodia Human Insulin ELISA kit (Mercodia, Cat #10-1113-01) and Human C-peptide ELISA kit (Mercodia, Cat #10-1141-01) was used to measure the insulin and C-peptide content in supernatant samples following manufacturer's protocols.

2.16. Western blotting

Cells were harvested at PP1 stages and lysed using cell lysis buffer containing protease inhibitors. Samples were separated on a 10% SDS-PAGE gel and transferred to PVDF Pre-Cut Blotting Membranes followed by blocking with 5% milk in Tris-based saline with Tween 20

(0.1% TBST) buffer for 1 h at R.T. The membrane was incubated with primary antibodies overnight at 4 °C, followed by incubation with HRP conjugated secondary antibodies at R.T. for 1 h. ECL western blotting detection reagent (Bio-rad, Cat #1705061) was used to visualize the protein bands. The following antibodies were used with the dilution ratio noted: goat anti-PDX1 (R&D, Cat #AF2419, 1:1,000), mouse anti-ACTB (b-Actin) (Cell Signaling Technology, Cat #3700S, 1:10,000).

2.17. Statistics

Statistical significance was determined using one-way ANOVA followed by Bonferroni's multiple comparisons test using GraphPad Prism (version 8.0.0 for Windows, GraphPad Software, San Diego, California USA). A value of $P < 0.05$ was considered statistically significant.

2.18. Accession numbers

Microarray, RNA-seq and ChIP-seq data has been submitted to the GEO database at NCBI under the accession number GSE125770.

3. RESULTS

3.1. Generation of β-like cells from patients carrying $PDX1^{P33T/+}$ and $PDX1^{C18R/+}$ mutations

To obtain samples from subjects with PDX1 mutations, 2547 participants of the Tübingen Family Study for T2D (TÜF study, currently more than 3000 participants, inclusion criteria given in Table 1) were screened by mass spectrometry for known rare mutations in the MODY4 gene PDX1 [33]. In this cohort, we identified six heterozygous P33T (Pro-Thr) carriers (frequency ~1:425) and one heterozygous C18R (Cys-Arg) carrier (frequency ~1:2500). Of note, both of the mutations occur at highly conserved amino acids in the transactivation domain of PDX1 (Suppl. Figure 1A,B). One of the PDX1 P33T carriers and the PDX1 C18R carrier were recruited for full-thickness skin biopsy, and primary dermal fibroblasts were isolated from the skin specimens. The clinical characteristics of the two mutation carriers compared to the average of the whole TÜF cohort showed decreased insulin secretion (Table 1). We reprogramed the primary fibroblasts into iPSCs using nucleofection with three episomal plasmids encoding human OCT4, SOX2, NANOG, LIN28, KLF4, and L-MYC (Suppl. Figure 1C) and several colonies were picked and expanded. The established control cell line XM001 as well as the P33T ($PDX1^{P33T/+}$) and C18R ($PDX1^{C18R/+}$) iPSC lines were reported previously [26,34,35].

To investigate the disease-relevant phenotype of these mutations during β-cell development, we differentiated patient-derived iPSCs into β-like cells using a differentiation protocol which is based on Rezania et al., 2014 (Figure 1A) [36]. Fluorescent activated cell sorting (FACS) analysis revealed approximately 90% positive cells for the definitive endoderm (DE) marker SOX17 (Suppl. Figure 2A-B). As expected, there was no difference between the patients and the control iPSC lines in endoderm differentiation, since PDX1 is not expressed until PP1 stage (Suppl. Figure 2C). Moreover, we detected ~85% PDX1-positive cells for all rounds of iPSC differentiation using FACS analysis at PP1 stage (Suppl. Figure 3A-C), while the protein levels of PDX1 were the same in cells derived from the patients (Suppl. Figure 3D-E). A similar differentiation efficiency was also observed for late stage PP2 where we detected ~40% PDX1/NKX6.1 double-positive cells derived from all iPSC cell lines by immunostaining and FACS analysis (Suppl. Figure 4A-C). Altogether, these data indicate that $PDX1^{P33T/+}$ and $PDX1^{C18R/+}$ mutations do not significantly impair early pancreatic progenitor differentiation.

Table 1 — Clinical characteristics of mutation carriers compared to the average of the TÜF study.

Trait	$PDX1^{P33T/+}$	$PDX1^{C18R/+}$		TÜF overall (N = 3029)
Gender	Female	Female	64.2% Females	
Age (yrs)	40	33	42	31—54
BMI (kg/m^2)	23.0^a	20.6^a	28.7	24.3—35.3
Body fat content (%)	29	24	33	24—45
Waist-hip ratio	0.819	0.766^a	0.869	0.813—0.941
Glucose$_0$ (mmol/L)	5.10	5.06	5.17	4.88—5.56
Glucose$_{120}$ (mmol/L)	5.83	4.90^a	6.22	5.28—7.33
HbA1c (%)	4.7^a	4.4^{a,b}	5.5	5.2—5.8
Insulin$_0$ (pmol/L)	39^a	40^a	68	42—112
Insulin$_{30}$ (pmol/L)	419	268^a	522	326—836
C-peptide$_0$ (pmol/L)	643	427	554	415—777
C-peptide$_{30}$ (pmol/L)	2372	1487	1824	1397—2407
Proinsulin$_0$ (pmol/L)	3	4	3	2—6
Proinsulin$_{30}$ (pmol/L)	12	16^a	8	4—13
AUC insulin$_{0-30}$/AUC glucose$_{0-30}$ (10^{-9})	28.8	25.7^a	43.6	28.5—66.7
AUC C-peptide$_{0-120}$/AUC glucose$_{0-120}$ (10^{-9})	340	266	288	237—356
HOMA-IR (10^{-6} mol*U*L^{-2})	1.47^a	1.50^a	2.61	1.57—4.47
ISI OGTT (10^{19} L^2*mol^{-2})	13.6	26.5^a	9.8	5.8—16.0
FFA (µmol/L)	519	618	566	434—720
Leukocytes (µl^{-1})	5140	2520^a	6080	5118—7380
CRP (mg/dL)	0.11	0.14	0.16	0.07—0.48
GOT (U/L)	18	18	21	17—27
GGT (U/L)	14	23	19	12—31
Triglycerides (mg/dL)	61^a	59^a	101	72—144
Total cholesterol (mg/dL)	164^a	190	191	167—217
HDL-cholesterol (mg/dL)	40^{a,b}	66^a	52	43—62
LDL-cholesterol (mg/dL)	106	122	113	94—137
TÜF inclusion criteria fulfilled	Previous GDM	FHD (one second-degree relative)	IFG and/or BMI ≥27 kg/m^2 and/or FHD and/or previous GDM	

TÜF data represent proportion (gender) or medians and interquartile ranges (all other traits). Subscript numbers indicate time-points (in minutes) of the oral glucose tolerance test.
^{a} Outside TÜF interquartile range.
^{b} Outside clinical reference range (central laboratory data). AUC — area under the curve; BMI — body-mass index; CRP — C-reactive protein; FFA — free fatty acids; FHD — family history of diabetes; GDM — gestational diabetes mellitus; GGT — γ-glutamyl transferase; GOT — glutamate-oxaloacetate transaminase; HbA1c — glycated hemoglobin A1c; HDL — high-density lipoprotein; HOMA-IR — homeostasis model assessment of insulin resistance; IFG — impaired fasting glycemia; ISI — insulin sensitivity index; LDL — low-density lipoprotein; OGTT — oral glucose tolerance test; TÜF — Tübingen Family study for type-2 diabetes.

To assess whether these two point mutations in *PDX1* affect late stages of β-cell development, we differentiated patient-derived iPSCs towards β-like cells. Immunostaining analysis revealed that both patients and control iPSCs generate predominantly cells, co-expressing C-peptide/NKX6.1 and C-peptide/PDX1, and minor populations expressing the α-cell hormone glucagon or the δ-cell hormone somatostatin (Figure 1B and Suppl. Figure 5A). Quantification of β-like cell differentiation efficiency showed ∼25% C-peptide-positive cells for the control but only ∼8% C-peptide-positive cells for the patient samples (Figure 1C,D). The transcript level of *INS* was lower in cells derived from the patients as revealed by q-PCR analysis (Figure 1E). The impairment in β-cell differentiation was also reflected by a weaker response to a glucose challenge in patient iPSCs-derived β-like cells compared to those derived from the control iPSCs, as assessed by a glucose-stimulated insulin secretion (GSIS) assay (Figure 1F and Suppl. Figure 5B). This reduced GSIS might be due to impaired β-cell glucose-responsive machinery components or delayed β-cell differentiation programs. Altogether, these data indicate that PDX1 heterozygous point mutations in the transactivation domain impair the differentiation of β-like cells and consequently impact their glucose-responsive function.

3.2. Characterization of $PDX1^{+/-}$, $PDX1^{P33T/P33T}$ and $PDX1^{C18R/C18R}$ mutations at the early pancreatic stage (PP1)

Although we analyzed two different patient-derived iPSC lines, it is possible that the observed phenotypes result from differences in the genetic background of control and the patient iPSC lines and are not due to the point mutations in the PDX1 transactivation domain. To exclude this possibility, we generated cell lines carrying homozygous *PDX1 P33T* ($PDX1^{P33T/P33T}$) and *C18R* ($PDX1^{C18R/C18R}$) point mutations from the control XM001 iPSC line. This approach also allowed us to analyze dose-dependent effects of the common *PDX1* mutations (Suppl. Figure 6A, C-D). Using targeted genetic modifications by the CRISPR/Cas9 system, we generated XM001 iPSC lines carrying $PDX1^{P33T/P33T}$ or $PDX1^{C18R/C18R}$ mutations. Furthermore, to study the effects of PDX1 haploinsufficiency, we generated a $PDX1^{+/-}$ XM001 iPSC line (Suppl. Figure 6B) by targeting the transactivation domain to generate a frame-shift mutation. Isogenic cells with *PDX1* haploinsufficiency or the point mutations on both alleles, displayed normal karyotype (Suppl. Figure 7A) and expressed pluripotency markers (TRA-1-81, SSEA-4, OCT3/4 and SOX2; Suppl. Figure 7B).

To address whether *PDX1* heterozygosity and homozygous point mutations affect pancreas development, we differentiated the isogenic control and mutant iPSCs towards the pancreatic lineage using an improved differentiation protocol by increasing the concentration of CHIR-99021 during S1 stage and adding IWP-2 during S2 stage. We found that all iPSC lines differentiated normally into endoderm cells co-expressing SOX17 and FOXA2 (∼90%) as determined by immunostaining and FACS analysis (Suppl. Figure 8A-C). At the PP1 stage, all control and mutant iPSC lines generated pancreatic progenitors with similar efficiency (∼90%) (Figure 2A—C), however, PDX1 protein levels (Figure 2D) as measured by FACS and immunofluorescence (Figure 2E,F) were substantially lower in PP1 cells differentiated from the $PDX1^{P33T/P33T}$ and $PDX1^{+/-}$ iPSCs as compared to the control and $PDX1^{C18R/C18R}$ iPSCs.
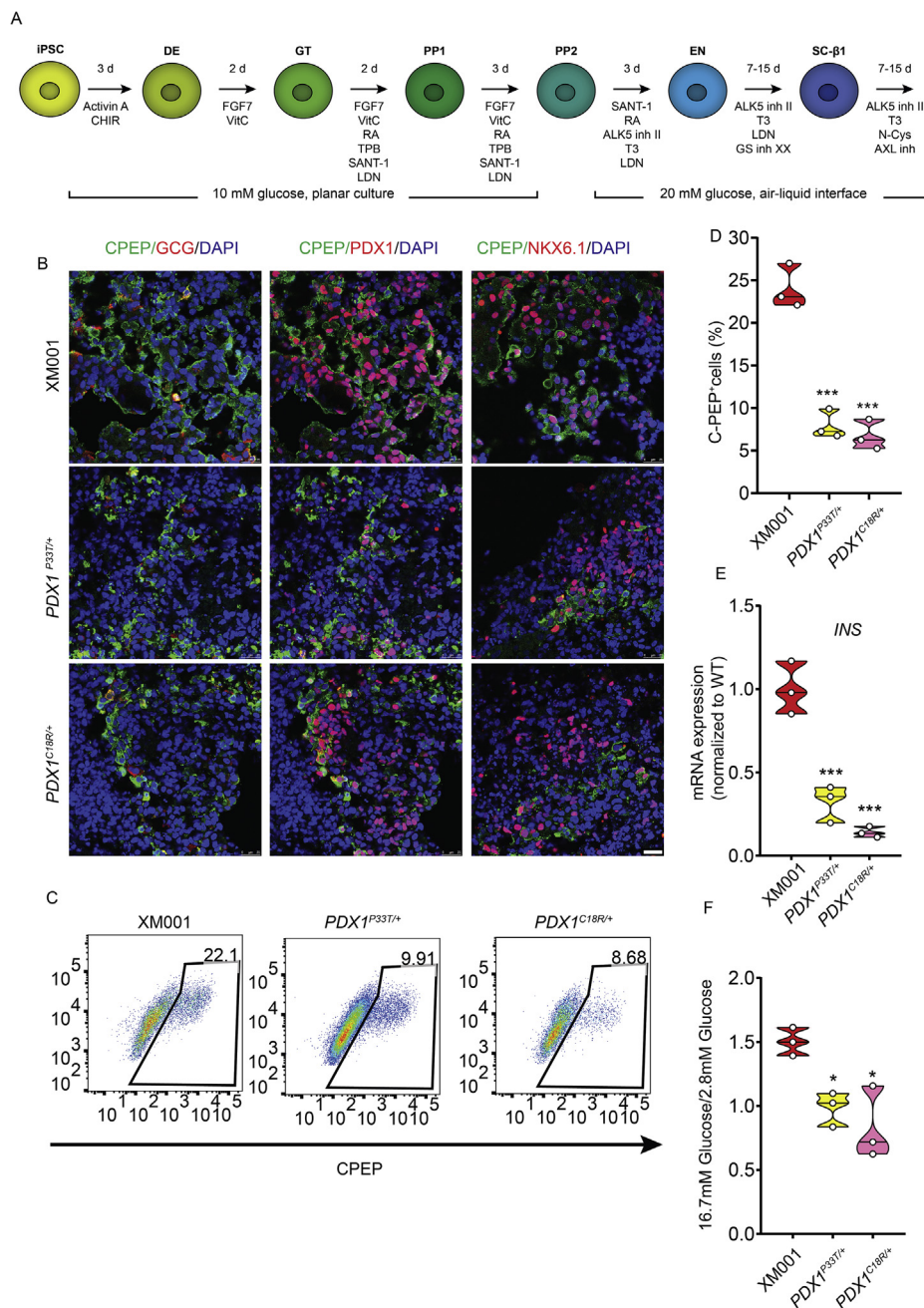
Figure 1: Generation of β-like cells from patients carrying *PDX1*$^{P33T/+}$ and *PDX1*$^{C18R/+}$ mutations. (A) Schematic of iPSC-derived β-like cells protocol. (B) Immunostaining for CPEP, GCG, PDX1, and NKX6.1 in the XM001, *PDX1*$^{P33T/+}$ and *PDX1*$^{C18R/+}$ cells at the S7 stage. Scale bar indicates 25 μm. (C) Representative FACS plots of CPEP$^+$ cells in the XM001, *PDX1*$^{P33T/+}$ and *PDX1*$^{C18R/+}$ cells at the S7 stage. (D) FACS quantification of the percentage of CPEP$^+$ cells in the XM001, *PDX1*$^{P33T/+}$ and *PDX1*$^{C18R/+}$ cells at the S7 stage (n = 3). (E) RT-qPCR analysis of *INS* gene expression in the XM001, *PDX1*$^{P33T/+}$ and *PDX1*$^{C18R/+}$ cells at the S7 stage (n = 3). (F) Glucose-stimulated insulin secretion assay for the XM001, *PDX1*$^{P33T/+}$, and *PDX1*$^{C18R/+}$ cells at the S7 stage. The fold change of insulin secretion with high glucose (16.7 mM) relative to low glucose (2.8 mM) treatment is shown (n = 3).

3.3. Characterization of *PDX1*$^{+/-}$, *PDX1*$^{P33T/P33T}$ and *PDX1*$^{C18R/C18R}$ mutations at the late pancreatic stage (PP2)

Although we detected PDX1 and NKX6.1 double-positive cells in all isogenic cell lines, the number of double-positive cells were significantly lower in *PDX1*$^{P33T/P33T}$ and *PDX1*$^{+/-}$ iPSC lines, as compared to *PDX1*$^{C18R/C18R}$ and control iPSC lines (Figure 3A—C), clearly demonstrating that the expression of *NKX6.1* and pancreatic differentiation into PP2 cells were impaired.

3.4. Characterization of the impact of *PDX1*$^{+/-}$, *PDX1*$^{P33T/P33T}$ and *PDX1*$^{C18R/C18R}$ mutations on β-like cell differentiation

To investigate the functional consequences of haploinsufficient PDX1 levels or homozygous *PDX1* point mutations in β-cell development, we differentiated isogenic iPSCs towards β-like cells. Similar to cells derived from the patient iPSCs, a majority of cells co-expressed C-peptide/NKX6.1 and C-peptide/PDX1 and only few cells expressed glucagon and somatostatin (Figure 4A and Suppl. Figure 9A). However,
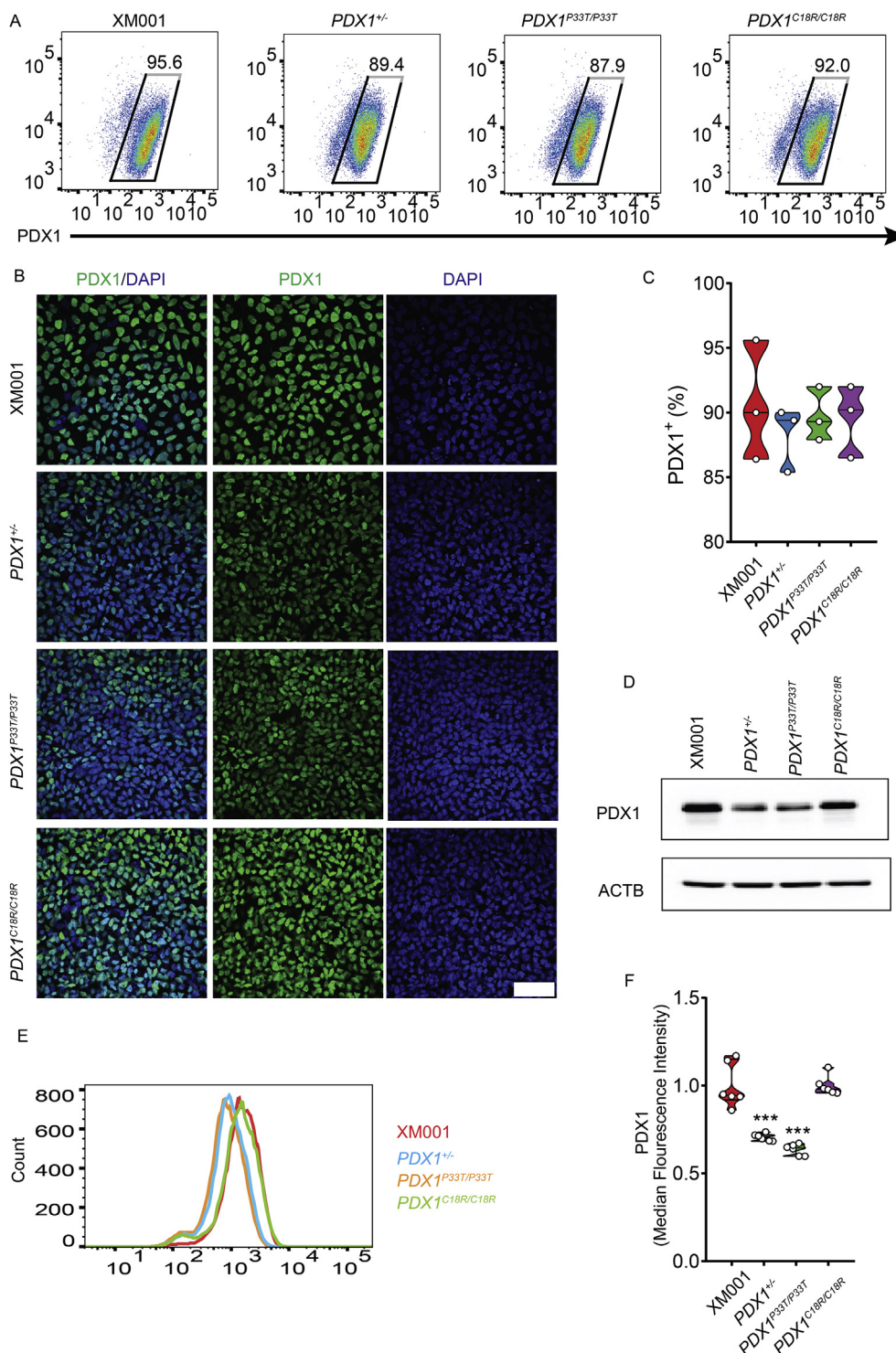
www.molecularmetabolism.com

Figure 2: Characterization of *PDX1*⁺/⁻, *PDX1*^P33T/P33T, and *PDX1*^C18R/C18R mutations at the early pancreatic stage (PP1). (A) Representative FACS plots of PDX1⁺ cells in XM001, *PDX1*⁺/⁻, *PDX1*^P33T/P33T, and *PDX1*^C18R/C18R cells at the early pancreatic stage. (B) Representative immunofluorescence staining of PDX1 in XM001, *PDX1*⁺/⁻, *PDX1*^P33T/P33T, and *PDX1*^C18R/C18R. Scale bar indicates 50 μm. (C) FACS quantification of the percentage of PDX1⁺ cells in XM001, *PDX1*⁺/⁻, *PDX1*^P33T/P33T and *PDX1*^C18R/C18R cells at the PP1 stage (n = 3). (D) Representative immunoblot of PDX1 expression from XM001, *PDX1*⁺/⁻, *PDX1*^P33T/P33T, and *PDX1*^C18R/C18R cells at the PP1 stage. (E) Representative FACS histograms comparing the differentiation efficiencies towards the PDX1⁺ cells in XM001, *PDX1*⁺/⁻, *PDX1*^P33T/P33T, and *PDX1*^C18R/C18R cells. (F) Median Fluorescence Intensity (MFI) quantification for XM001, *PDX1*⁺/⁻, *PDX1*^P33T/P33T, and *PDX1*^C18R/C18R cells at the PP1 stage stained with PDX1 antibody (n = 6).
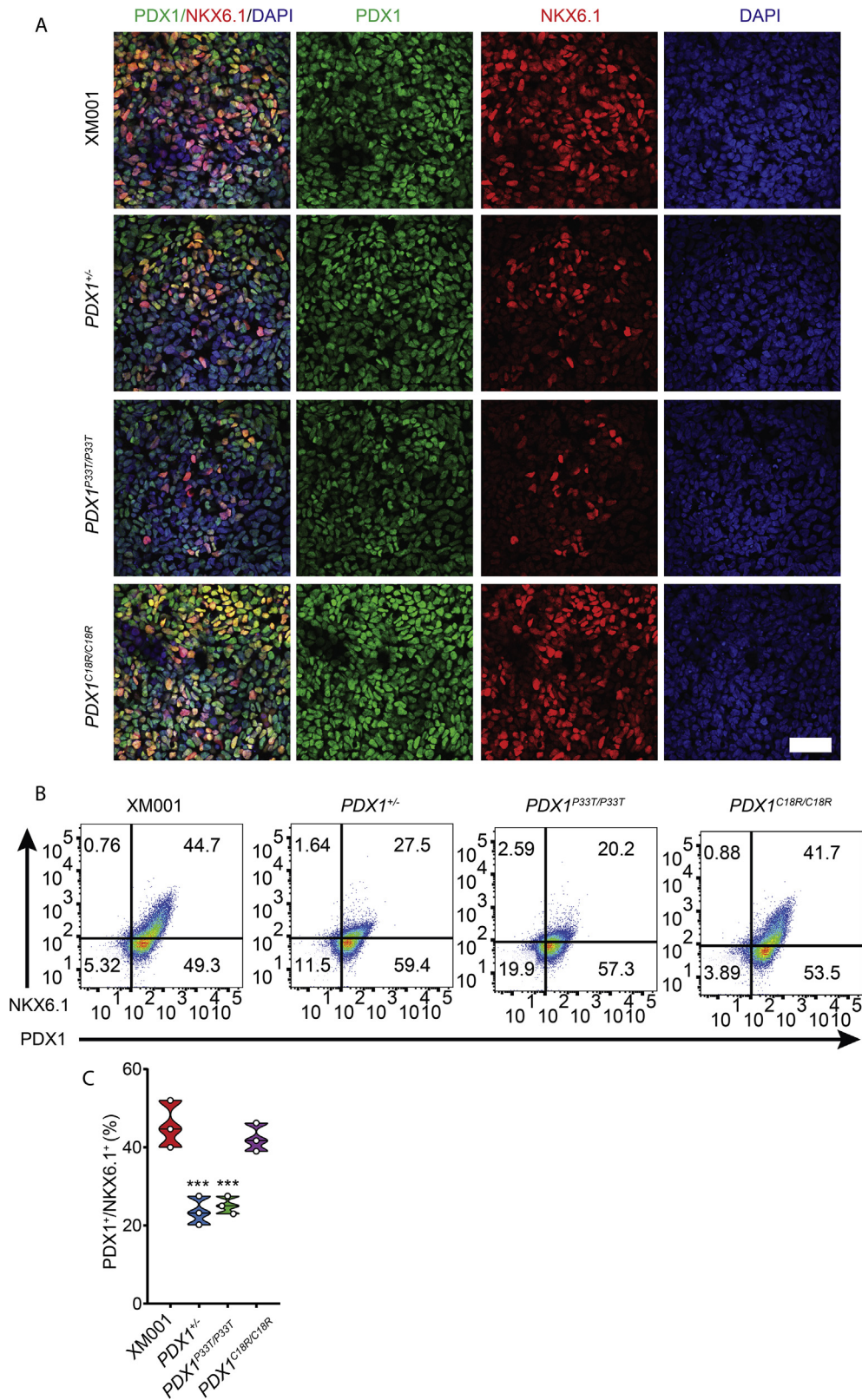
Figure 3: Characterization of _PDX1_$^{+/-}$, _PDX1_$^{P33T/P33T}$ and _PDX1_$^{C18R/C18R}$ mutations at the late pancreatic stage (PP2). (A) Representative immunofluorescence staining of PDX1 and NKX6.1 in XM001, _PDX1_$^{+/-}$, _PDX1_$^{P33T/P33T}$, and _PDX1_$^{C18R/C18R}$ cells. Scale bar indicates 50 μm. (B) Representative FACS plots of PDX1$^+$ and NKX6.1$^+$cells in XM001, _PDX1_$^{+/-}$, _PDX1_$^{P33T/P33T}$, and _PDX1_$^{C18R/C18R}$ cells at the PP2 stage. (C) FACS quantification of the percentage of PDX1$^+$ and NKX6.1$^+$cells in XM001, _PDX1_$^{+/-}$, _PDX1_$^{P33T/P33T}$, and _PDX1_$^{C18R/C18R}$ cells at the PP2 stage (n = 3).

the number of total C-peptide-positive cells, monohormonal C-peptide-positive cells and cells expressing both C-peptide and NKX6.1 derived from $PDX1^{+/-}$ and $PDX1^{P33T/P33T}$ and $PDX1^{C18R/C18R}$ mutant isogenic iPSC lines were less compared to the control (Figure 4B–D and Figure 5A,B).

3.5. *PDX1* mutations reduce glucose-responsive function of β-like cells

Furthermore, we performed functional analysis of isogenic iPSC-derived β-like cells using GSIS that revealed a significant impairment in the response to glucose in cells derived from the isogenic mutants compared to the control cells (Figure 5C and

Suppl. Figure 9B). To explain how *PDX1* mutations cause defects in β-like cell function, we performed q-PCR analysis of differentiated endocrine cells. The transcript levels of *INS* and *SST* but not *GCG* were lower in cells derived from $PDX1^{+/-}$ and $PDX1^{C18R/C18R}$ compared to the control and the transcript levels of *INS*, *SST*, and *GCG* were lower in cells derived from $PDX1^{P33T/P33T}$ (Figure 5D). We also found lower expression levels of *NEUROD1*, *ISLI*, *ABCC8*, and *UCN3* in cells derived from all isogenic mutations. Importantly, the expression levels of *PDX1*, *NKX6-1*, *MAFA*, *PAX6*, *SLC30A8*, and *KCNJ11* were less in the $PDX1^{+/-}$ and $PDX1^{P33T/P33T}$ iPSCs-derived β-like cells but not in those originated from the $PDX1^{C18R/C18R}$ (Figure 5D), highlighting distinct effects on gene expression of different mutations in *PDX1*. Of note, with the
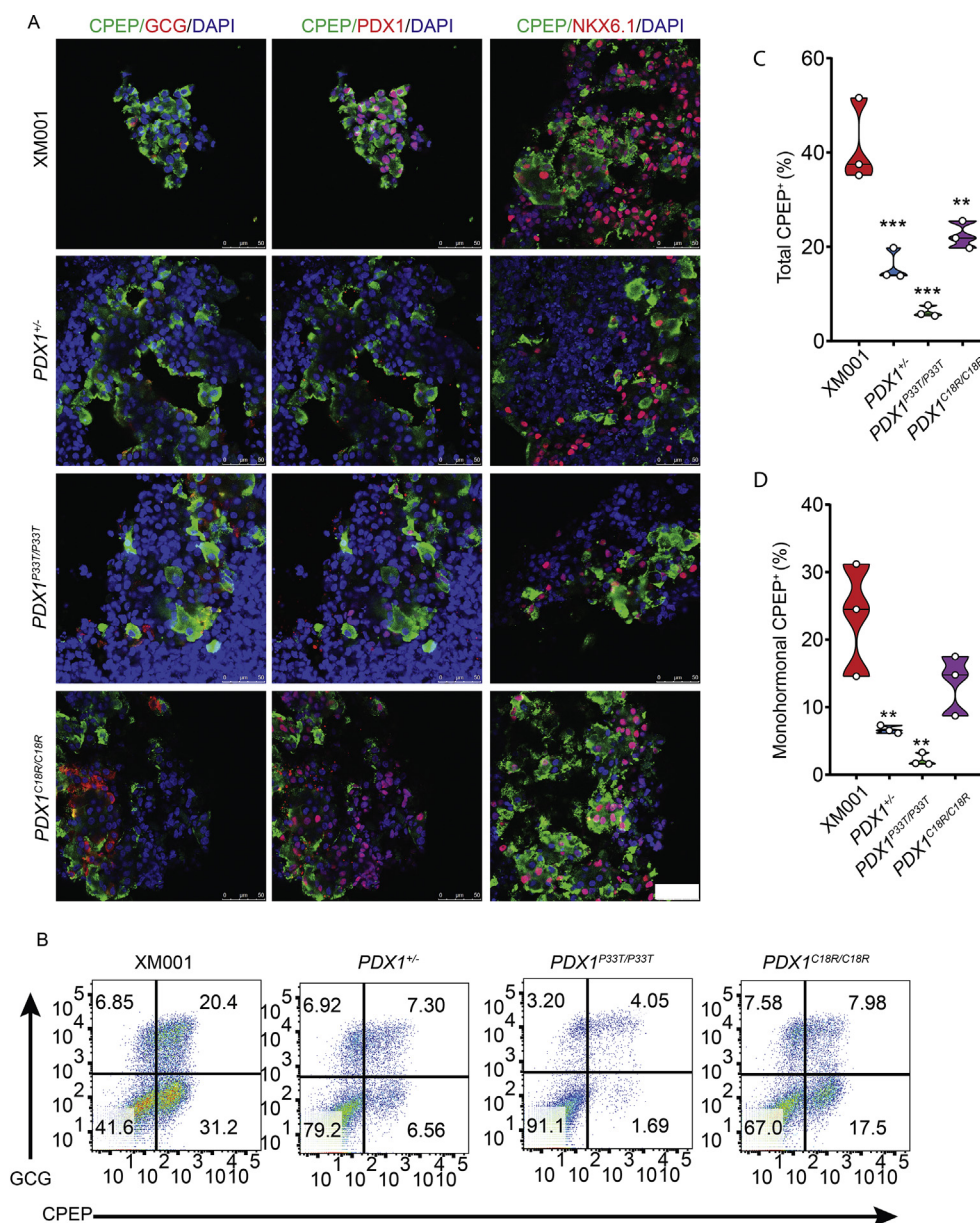

Figure 4: Characterization of the impact of $PDX1^{+/-}$, $PDX1^{P33T/P33T}$, and $PDX1^{C18R/C18R}$ mutations on β-like cell differentiation. (A) Representative immunofluorescence staining for C-peptide, Glucagon, PDX1 and NKX6.1 in XM001, $PDX1^{+/-}$, $PDX1^{P33T/P33T}$, and $PDX1^{C18R/C18R}$ cells at the S7 stage. Scale bar indicates 50 μm. (B) Representative FACS plots of CPEP$^+$ and GCG$^+$ cells in XM001, $PDX1^{+/-}$, $PDX1^{P33T/P33T}$, and $PDX1^{C18R/C18R}$ cells at the S7 stage. (C) FACS quantification of the percentage of total CPEP$^+$ cells in the XM001, $PDX1^{+/-}$, $PDX1^{P33T/P33T}$, and $PDX1^{C18R/C18R}$ cells at the S7 stage (n = 3). (D) FACS quantification of the percentage of mono-hormonal CPEP$^+$ cells in the XM001, $PDX1^{+/-}$, $PDX1^{P33T/P33T}$, and $PDX1^{C18R/C18R}$ cells at the S7 stage (n = 3).

† Bound by PDX1 in XM001 PPs
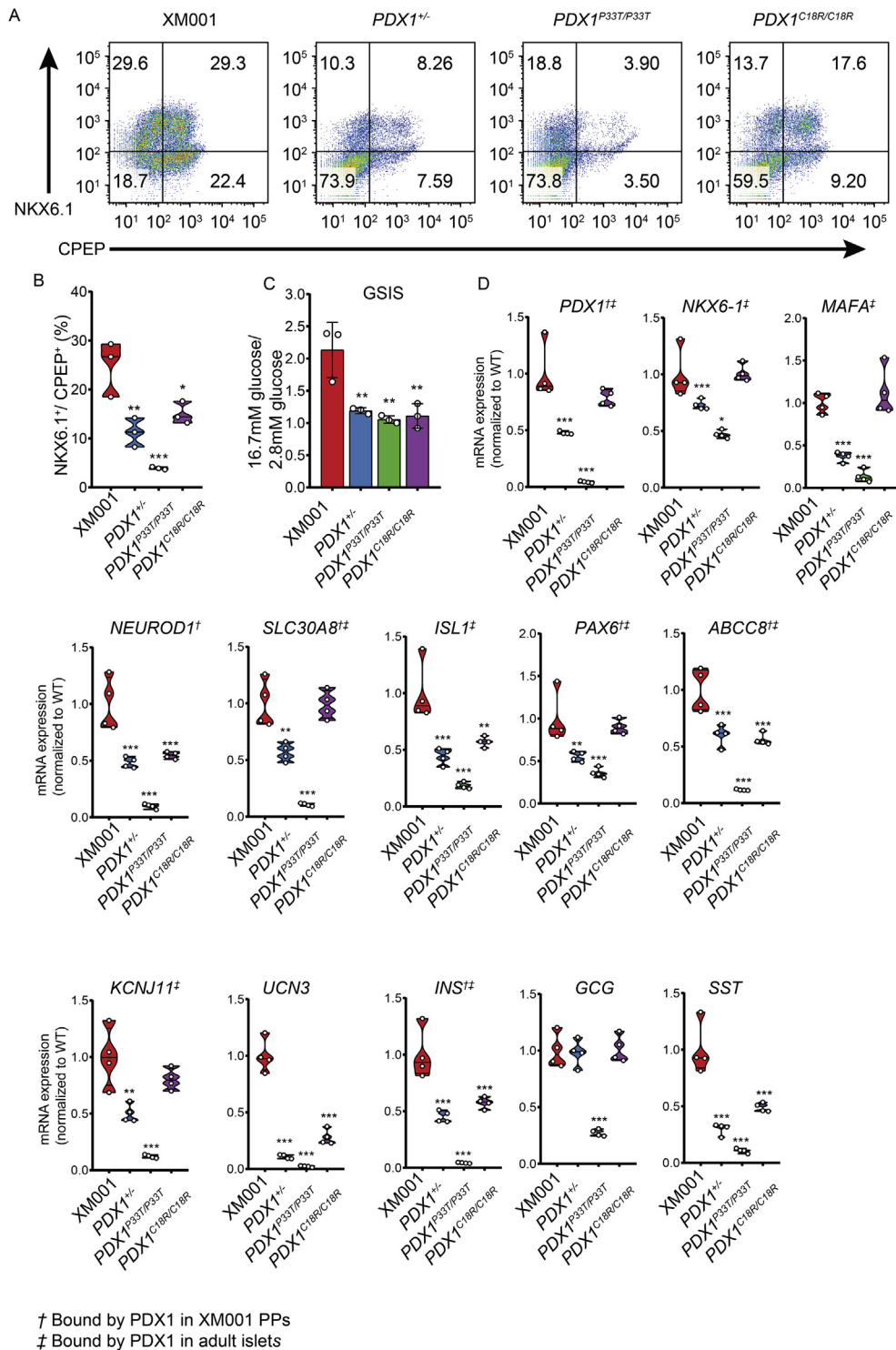‡ Bound by PDX1 in adult islets

Figure 5: *PDX1* mutations reduce glucose-responsive function of β-like cells. (A) Representative FACS plots for C-peptide⁺ and NKX6.1⁺ in XM001, *PDX1⁺ᐟ⁻*, *PDX1^P33T/P33T* and *PDX1^C18R/C18R* cells at the S7 stage. (B) FACS quantification of the percentage of total CPEP⁺ and NKX6.1⁺ cells in the XM001, *PDX1⁺ᐟ⁻*, *PDX1^P33T/P33T*, and *PDX1^C18R/C18R* cells at the S7 stage (n = 3). (C) GSIS assay for the XM001, *PDX1⁺ᐟ⁻*, *PDX1^P33T/P33T*, and *PDX1^C18R/C18R* cells at the S7 stage. The fold change of insulin secretion with high glucose (16.7 mM) relative to low glucose (2.8 mM) treatment is shown (n = 3). (D) RT-qPCR analysis of expression of β-cell transcription factors, hormonal markers and β-cell functional markers at the S7 stage (n = 4).

exception of *UCN3*, *GCG*, and *SST*, all tested genes are bound by PDX1 in either adult islets (high confidence PDX1 binding sites [26]), XM001 PP1 cells [26] or both (Figure 5D). These data indicate that point

mutations in the transactivation domain reduce the potential of the PDX1 TF to activate the expression of its target genes during β-like cell development and maturation. Furthermore, the *PDX1^P33T/P33T* mutation

causes greater impact on β-like cell formation and function than the $PDX1^{C18R/C18R}$ mutation.

3.6. RNA-seq profiling of pancreatic progenitors (PP1) from $PDX1^{+/−}$, $PDX1^{P33T/P33T}$ and $PDX1^{C18R/C18R}$ iPSC lines

To identify the immediate early PDX1 target genes, which react to haploinsufficiency and the homozygous point mutations in the trans-activation domain and which could explain the impaired PP2 differentiation, we performed RNA-seq at the PP1 stage. As quality control, we compared control iPSCs at pluripotency to the average of all other tested cell lines at PP1 stage and, as expected, identified upregulation of a pancreatic gene program (*PDX1*, *HNF1B*, *SOX9*, *ONECUT1*, *HHEX*, *FOXA2*, and *RFX6*) as well as downregulation of a pluripotency program (Figure 6A,B). Furthermore, principal component analysis (PCA) showed two distinct clusters along the first principal component, corresponding to control iPSCs and the different PPs. Moreover, the second principal component separates the $PDX1^{+/−}$, $PDX1^{P33T/P33T}$, and $PDX1^{C18R/C18R}$ PPs from XM001 control PPs and shows that $PDX1^{+/−}$ and $PDX1^{P33T/P33T}$ are more similar to each other compared to $PDX1^{C18R/C18R}$ and control cells (Figure 6C). Next, we compared mRNA profiles from PP1 cells with isogenic *PDX1* mutation to control PP1 cells. When compared to the control PPs, we found 112, 196 and 199 deregulated genes in $PDX1^{+/−}$, $PDX1^{P33T/P33T}$, and $PDX1^{C18R/C18R}$ PPs, respectively. Among these, 20, 41, and 54 genes were bound by PDX1, respectively (Figure 6D—F). Interestingly, we found the diabetes risk genes *LARGE1* and *ANPEP* and insulin resistance genes *MEG3* and *CES1* to be consistently downregulated among all PPs with *PDX1* mutations (Figure 6G). Moreover, genes such as the metabolic disease
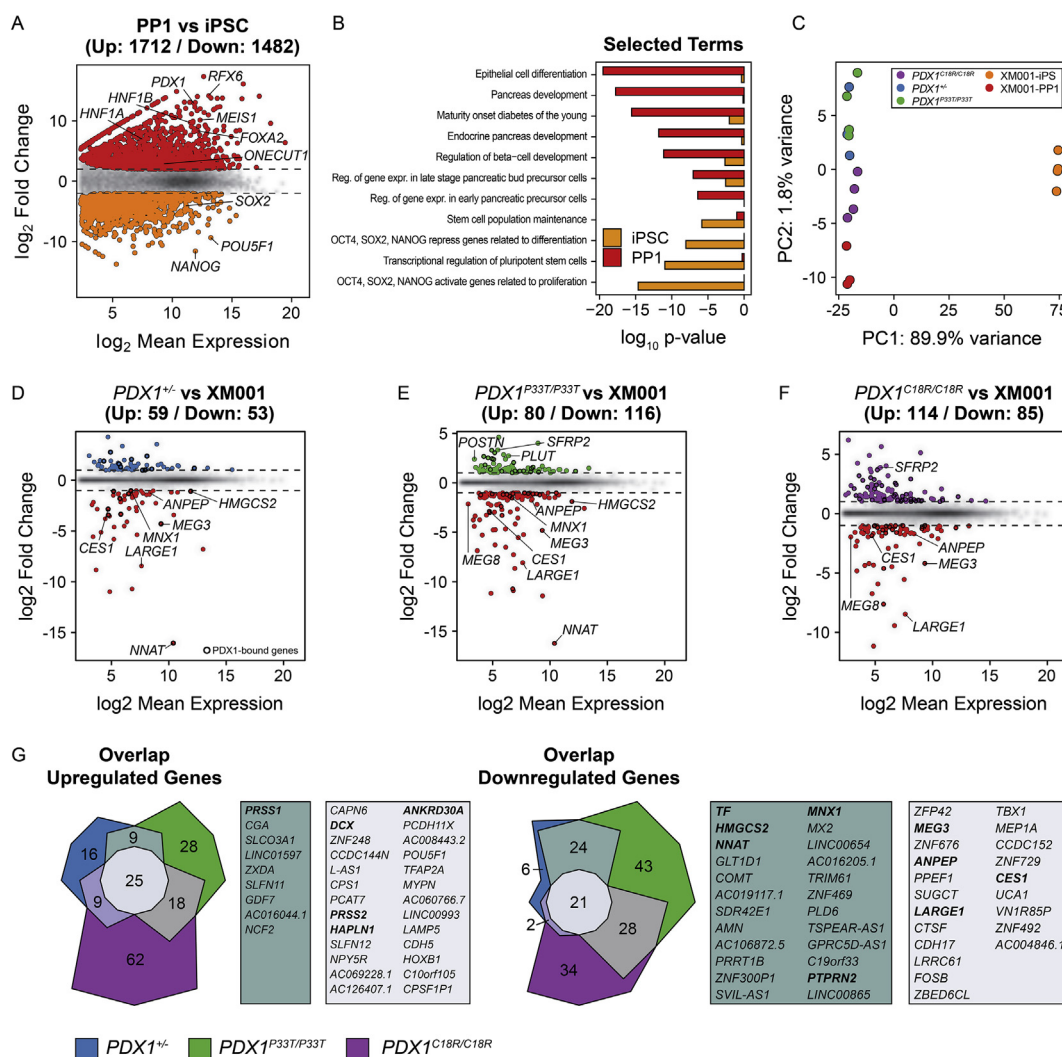

Figure 6: RNA-seq profiling of pancreatic progenitors (PP1) from $PDX1^{+/−}$, $PDX1^{P33T/P33T}$, and $PDX1^{C18R/C18R}$ iPSC lines. (A) MA plot showing the mean $\log_2$ expression against the $\log_2$-fold change of the RNA-Seq data obtained from XM001 iPSCs and PPs from XM001 and isogenic *PDX1* mutants. Genes with significantly different expression ($\log_2$ fold change ≥ 2 and adjusted p-value ≤ 0.05) are drawn in color. Red depicts increased expression in PPs, whereas orange depicts increased expression in iPSCs. (B) Bar graph of p-values from pathway enrichment analysis, showing selected GO terms and KEGG and Reactome pathways from differentially expressed genes. (C) Principal component analysis (PCA) of iPSCs and PP1 cells. (D—F) MA plots showing the mean $\log_2$ expression against the $\log_2$ fold change of the RNA-Seq data obtained from $PDX1^{+/−}$, $PDX1^{P33T/P33T}$, and $PDX1^{C18R/C18R}$ compared to XM001. Genes with significantly different expression ($\log_2$ fold change ≥ 1 and adjusted p-value ≤ 0.1) are drawn in color. Red depicts increased expression in XM001 control PPs, blue, green and purple depict increased expression in $PDX1^{+/−}$, $PDX1^{P33T/P33T}$, and $PDX1^{C18R/C18R}$, respectively. Black circles genes with PDX1 binding sites in XM001 PPs. (G) Venn diagrams showing the overlap of up- and downregulated genes from $PDX1^{+/−}$, $PDX1^{P33T/P33T}$, and $PDX1^{C18R/C18R}$ PPs compared to XM001 PPs. Some relevant pancreatic and disease associated genes are set in bold.

associated genes *HAPLN1*, the β-cell hallmark gene *DCX*, the fibro-calculous pancreatic diabetes associated genes *PRSS1/2*, which are the main contributors to the difference between PPs from mutant and control isogenic cell lines, were consistently deregulated (Suppl. Figure 10). Since PDX1 levels are reduced in *PDX1*$^{P33T/P33T}$ PPs, we compared the downregulated genes with those from *PDX1*$^{+/-}$ PPs. Among these genes, we found the transcription factor *MNX1* and the proteolipid *NNAT*, as well as genes that seem to distinguish *PDX1*$^{P33T/P33T}$ and *PDX1*$^{+/-}$ from *PDX1*$^{C18R/C18R}$ and XM001 PPs like *TF* and *METTL9* (Figure 6D,E and G and Suppl. Figure 10).

3.7. Characterization of PDX1 binding in patient-derived *PDX1*$^{P33T/+}$ pancreatic progenitors (PP1)

Since the *PDX1*$^{P33T/P33T}$ mutation in isogenic cells severely reduced PP2 cell differentiation and the *PDX1*$^{P33T/+}$ patient was diagnosed with gestational diabetes, we sought to identify genes that might be differentially regulated due to the heterozygous expression of the P33T allele. To this end, we first differentiated iPSCs from the *PDX1*$^{P33T/+}$ patient and the control iPSC into PP1 using the 2nd differentiation protocol. To understand whether the heterozygous P33T mutation affects PDX1 DNA-binding activity, we employed ChIP-seq analysis to profile genome-wide PDX1 binding sites in control [26] and *PDX1*$^{P33T/+}$ patient iPSC-derived PPs. We identified 8970 PDX1 binding sites in the patient iPSC-derived PP cells that were predominantly found in inter-genic and intronic regions and showed a clear enrichment at pro-moters and 5' UTRs (Figure 7A,B and Suppl. Figure 11A-B). Motif analysis showed that 71% of the binding sites harbor a PDX1 consensus sequence, confirming the high quality of our data (Figure 7C). Moreover, ChIP-seq of the active histone modification H3K27ac in control [26] and patient-derived PPs showed a ∼5 fold enrichment of H3K27ac at the PDX1-bound sites (Figure 7D and Suppl. Figure 11C). Compared to the ChIP-seq data from control PP
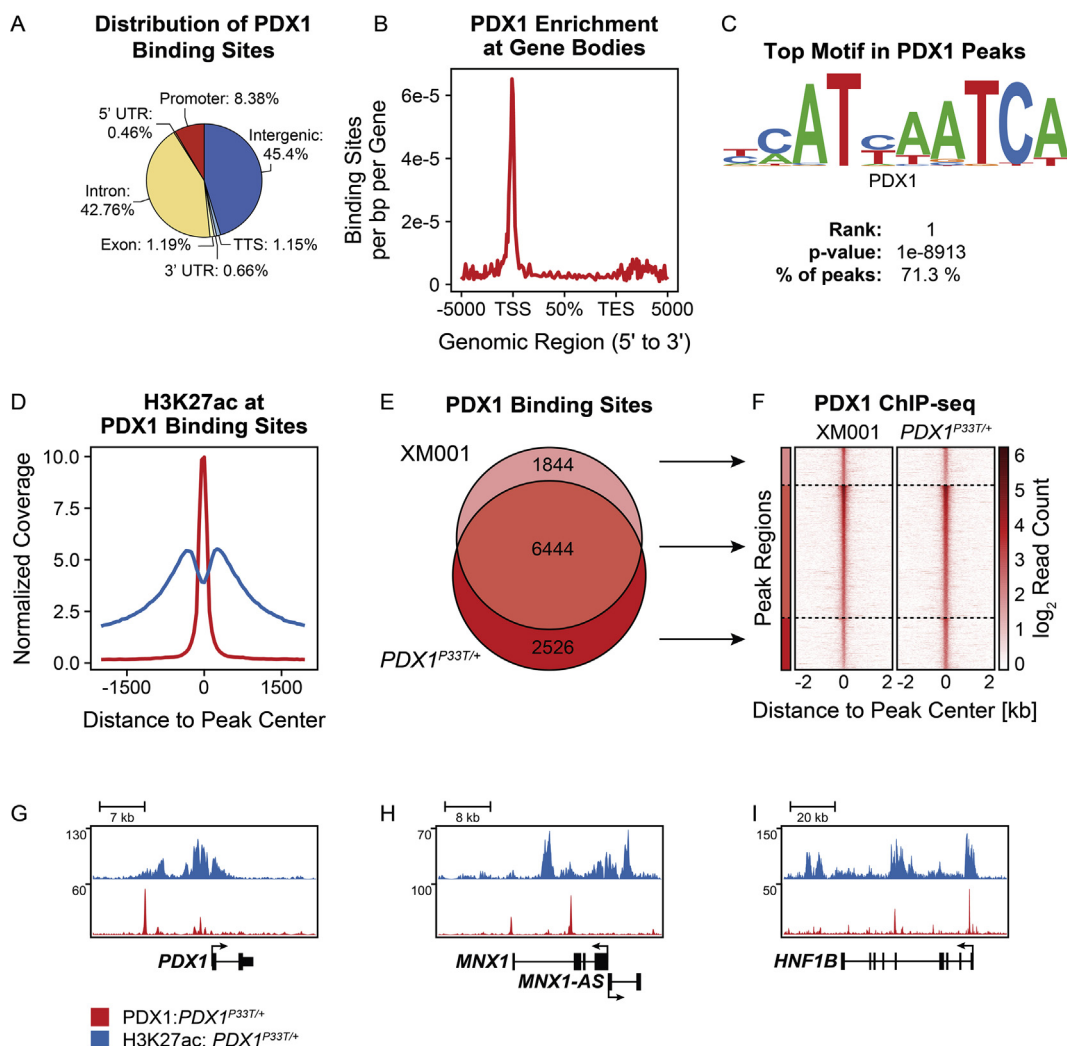

Figure 7: Characterization of PDX1 binding in patient-derived *PDX1*$^{P33T/+}$ pancreatic progenitors (PP1). (A) Distribution of PDX1 binding sites among genomic features. PDX1$^{P33T/+}$ binds predominantly to intergenic, intronic and promoter regions. (B) Meta-genomic plot showing the enrichment of PDX1 at the transcriptional start sites (TSS) of its target genes displayed as binding sites per base pair (bp) per gene over the genomic regions of all RefSeq genes. (C) Most enriched motif detected by motif analysis resembles the known PDX1 consensus sequence and is identified in 71.3% of all PDX1-bound sequences. (D) Average ChIP-seq Signal of H3K27ac (blue) and PDX1 (red) at PDX1 binding sites shows enrichment of H3K27ac at PDX1-bound sites. (E) Venn diagram showing the overlap of PDX1-binding sites in XM001 PPs and *PDX1*$^{P33T/+}$ PPs. (F) Heatmap of PDX1 ChIP-seq signal at all PDX1 binding sites in XM001 and *PDX1*$^{P33T/+}$ PPs, showing high resemblance of PDX1 binding in these cells. (G) ChIP-seq data tracks showing the enrichment of H3K27ac (blue) and PDX1 (red) at the loci of important pancreatic genes.

cells [26], we did not find pronounced differences in PDX1 binding or H3K27ac enrichment in cells derived from the patient compared to the control (Figure 7E,F and Suppl. Figure 11D-K). Of the 8970 PDX1 binding sites in the patient, 6444 are shared with the control PPs (Figure 7E). Next, we mapped PDX1 binding sites, shared between the control and $PDX1^{P33T/+}$ PPs, to genes and identified 3978 potential target genes. Among those, we found important pancreatic genes such as $PDX1$, $MNX1$, or $HNF1B$ (Figure 7G—I).

3.8. mRNA profiles of patient-derived $PDX1^{P33T/+}$ pancreatic progenitors (PP1)

Furthermore, microarray analysis of control [26] and patient-derived $PDX1^{P33T/+}$ cells was performed at the pluripotency and PP stages. A total of 2370 differentially expressed genes were identified between

iPSC and PP (FC $\geq$ 2, FDR $\leq$ 5%). Important pancreatic genes including $HNF1B$, $SOX9$, $ONECUT1$, and $HHEX$ were found to be upregulated in PPs. In contrast, pluripotency associated genes such as $NANOG$ and $LIN28A$ were specifically expressed in the iPSC stage (Figure 8A). Functional analysis of deregulated genes by means of GO term and pathway enrichment showed that genes upregulated in PPs were associated with pancreas development while downregulated genes were linked to embryonic stem cell, cell cycle and proliferation (Figure 8B). Comparing the transcriptional profile of PPs from $PDX1^{P33T/+}$ with controls, we identified 88 deregulated genes (FC $\geq$ 2, FDR $\leq$ 5%), among which 21 genes possessed PDX1 binding sites (Figure 8C). Remarkably, we identified downregulation of $MEG3$ and $NNAT$ genes, which have PDX1 binding sites and are involved in pancreas development and insulin secretion. Importantly, we also
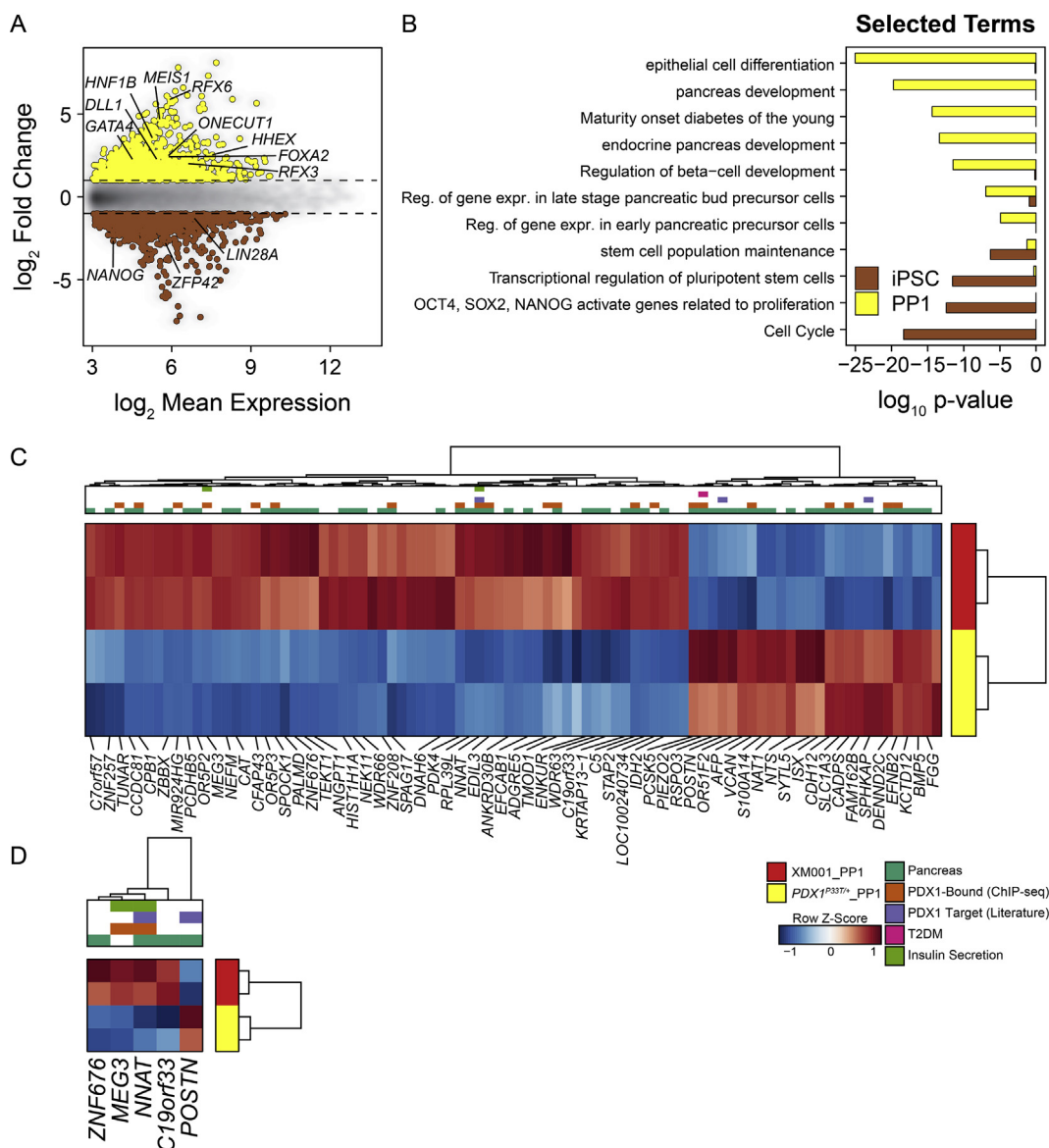

Figure 8: mRNA profiles of patient-derived $PDX1^{P33T/+}$ pancreatic progenitors (PP1). (A) MA plot showing the mean log$_2$ expression against the log$_2$-fold change of the microarray data obtained from XM001 iPSCs and PPs. Genes with significantly different expression (log$_2$ fold change $\geq$ 1 and adjusted p-value $\leq$ 0.1) are drawn in color. Yellow depicts increased expression in PPs, whereas brown depicts increased expression in iPSCs. (B) Bar graph of p-values from pathway enrichment analysis, showing selected GO terms and KEGG and Reactome pathways from differentially expressed genes. (C) Heatmap of differentially expressed genes between patient-derived $PDX1^{P33T/+}$ and XM001 control PPs. (D) Heat map and clustering showing consistently deregulated genes in patients $PDX1^{P33T/+}$ and isogenic $PDX1^{P33T/P33T}$ PPs.

Original Article

identified a set of genes showing consistent deregulation between $PDX1^{P33T/P33T}$ PPs and patient derived $PDX1^{P33T/+}$ PPs that include *NNAT*, *MEG3*, and *POSTN* (Figure 8D). Intriguingly, Periostin, which is encoded by the *POSTN* gene, is involved in pancreas and β-cell regeneration [37], and both *NNAT* and *MEG3* are associated with insulin secretion.

4. DISCUSSION

The translation of findings from successful preclinical reports from animal models to human often fail due to the evolutionary diversity in organ development and function among species. In this context, discovering novel treatments for diabetes mellitus necessitates comprehensive understanding of the mechanisms underlying human endocrine cell formation, function and failure. Due to the limited access to human primary samples and the unfeasibility of performing longitudinal analyses in humans, the establishment of novel modeling systems to study human pancreas homeostasis is essential [38]. Along these lines, *in vitro* differentiation of β-cells from stem cells provides a unique platform to study human endocrine cell development and to model human disease [36,39,40]. In particular, this system enables the study of defects in developmental programs, leading to an increased predisposition to diabetes, by mimicking the phenotypes of mutations in specific genes such as those associated with MODY. Uncovering the consequence of such mutations will aid to identify the carrier individuals and design personalized prevention and treatment approaches, as has been shown for sulfonylurea treatment for patients carrying *KCNJ11* mutation in the potassium channel [41].

Here, using iPSCs endocrine differentiation culture, we investigated the impact of two common heterologous mutations (P33T, C18R) in the *PDX1* gene on human β-cell development and function. Using iPSCs from glucose intolerant patients as well as newly generated isogenic cell lines, we found that these mutations impair endocrine progenitor and β-cell development. However, our data revealed $PDX1^{P33T/+}$ and $PDX1^{C18R/+}$ mutations in patient-derived cells do not affect early stages of pancreatic differentiation. In comparison, $PDX1^{P33T/P33T}$ impaired the induction of endocrine fate at the PP2 stage, suggesting a dose-dependent effect of the P33T mutation on the endocrine lineage decision. Importantly, the levels of PDX1 protein were reduced at the PP1 stage in cells carrying a homozygous P33T mutation. In mouse, it has been shown that Pdx1 can regulate its own expression through an auto-regulatory positive feedback mechanism [42–44]. As the P33T mutation lies in the transactivation domain of PDX1, it is tempting to speculate that this mutation weakens protein–protein interactions and impairs the recruitment of transcriptional co-activators required for the induction of target gene expression and *PDX1* itself. Interestingly, in the $PDX1^{P33T/P33T}$ mutant PP cells, the lncRNA *PLUTO* is upregulated. *PLUTO*, which is downregulated in T2D, regulates *PDX1* expression by promoting interactions between the *PDX1* promoter and an upstream enhancer cluster [45], suggesting that its upregulation in $PDX1^{P33T/P33T}$ mutant PPs is due to a compensatory mechanism aiming to increase *PDX1* expression. The reduction in PDX1 levels at PP1 stage coincided with the impaired PP2 differentiation. During endocrinogenesis, the maintenance of high levels of PDX1 is essential for induction and differentiation of endocrine progenitors [46]. Therefore, the reduced levels of PDX1 likely hamper endocrine fate specification in human $PDX1^{P33T/P33T}$ mutant progenitors, supporting an evolutionary conserved mechanism of PDX1 function during endocrine cell differentiation. Interestingly, $PDX1^{C18R/C18R}$ mutation reduced neither PDX1 levels at PP1 stage nor at PP2 cell development. This difference between the effects of the two mutations might be due to the more severe changes in protein

structure, induced by the replacement of proline with threonine in P33T mutation. Proline is the major amino acid generating tight turns in protein sequences and its replacement with any other amino acid might result in significant changes in transactivation domain structure and protein–protein interactions. Therefore, it is likely that changing proline to threonine in PDX1 reduces its interaction with co-binding transcription factors. This is also supported by the similar phenotype of cells carrying $PDX1^{P33T/P33T}$ mutation and those carrying $PDX1^{+/-}$, suggesting a significant loss-of function upon this point mutation. However, at least in the $PDX1^{P33T/P33T}$ and $PDX1^{+/-}$ isogenic cell lines, the reduced expression of PDX1 might cause binding patterns to change, since it is possible that the remaining amount of PDX1 is not sufficient to activate low affinity binding sites.

Gene expression analysis from PPs derived from patient and isogenic cells carrying $PDX1^{P33T/+}$ and $PDX1^{P33T/P33T}$, identified downregulation of several PDX1 target genes including *MEG3* and *NEURONATIN* (*NNAT*). Maternally expressed gene 3 (*Meg3*) is an imprinted gene, coding for a long noncoding RNA, that resides in the distal region of mouse chromosome 12, and its human homolog is located in the syntenic region on chromosome 14. In mouse, the downregulation of Meg3 affects insulin synthesis and secretion in pancreatic β-cells [47]. Furthermore, this gene is downregulated in islets from T2D, suggesting an essential role for β-cell development and/or function [48]. *NNAT* is an imprinted gene coding for the proteolipid *NEURONATIN*, is expressed in neuroendocrine and metabolic tissues in a hormone- and glucose-sensitive manner. Rare single-nucleotide polymorphisms (SNPs) at the human *NNAT* locus are associated with extreme childhood obesity [49]. Mice lacking *Nnat* specifically in β-cells, exhibit reduced insulin content and impaired GSIS, demonstrating its involvement in regulation of glucose homeostasis and insulin secretion [50]. However, a function of this protein in pancreatic developmental has not been reported so far; therefore, it will be exciting to explore whether *NNAT* influences human β-cell development. Moreover, PPs derived from all isogenic mutants exhibited downregulation of common genes, i.e. *MEG3*, *LARGE1*, *ANPEP*, and *CES1*. It has been shown that mutations in *LARGE1* might increase the risk of type 2 diabetes through accumulation of visceral fat and increased insulin resistance [51]. In the *ANPEP* locus, SNPs influencing the expression of the *ANPEP* gene, coding for the aminopeptidase N, are associated with an increased risk of T2D [52]. Furthermore, global $Ces1^{-/-}$ mice have shown elevated plasma levels of triglycerides, free cholesterol, FFAs, and insulin, and displayed insulin resistance [53]. However, whether *LARGE1*, *ANPEP*, and *CES1* play a role during human β-cell development and/or function needs further investigation. In addition, we detected the downregulation of *MNX1* in $PDX1^{P33T/P33T}$ PPs. In mouse, this TF promotes and maintains the β-cell program during embryonic and postnatal stages, respectively, thereby regulating endocrine lineage allocation and β-cell fate maintenance [54]. Although homozygous *MNX1* mutation causes permanent neonatal diabetes in humans [55], the mechanisms by which this protein impacts human β-cell development still need to be addressed.

Both $PDX1^{P33T/P33T}$ and $PDX1^{C18R/C18R}$ mutations deteriorated β-cell development and function. We found the downregulation of several key TFs regulating β-cell differentiation such as *NEUROD1* and *ISLI* upon homozygous single base-pair mutations. These data indicate that PDX1 fails to activate these target genes upon point mutations and further highlight the essential role of this TF for human β-cell development. Of note, we found significant reduction in the expression levels of *UCN3* in cells expressing homozygous PDX1 mutants, underlining the importance of proper PDX1 function for β-cell maturation, similar to rodents. Recently, we have shown that impairment in Pdx1 TF activity in double

knock-in reporter mice reduces β-cell maturation in male mice and leads to diabetes, whereas female animals are protected until pregnancy when they develop gestational diabetes [56,57]. Due to the report on gestational diabetes in the $PDX1^{P33T/+}$ patient and the reduction in $UCN3$ levels in β-like cells carrying this mutation, it is likely that β-cells from this patient function sub-optimally, which becomes evident upon metabolic demand similar to the above described mouse model. These results suggest an evolutionary conserved function for PDX1 in regulating β-cell maturation and function.

The differentiated β-cells carrying $PDX1$ point mutations were less functional compared to WT cells in term of glucose responsiveness. In mouse, Pdx1 is known to regulate GSIS. This TF not only directly regulates insulin synthesis, but also induces the expression of secretory machinery components required for insulin release [11]. We showed the downregulation of INS, $ABCC8$, $KCNJ11$, and $SLC30A8$ upon $PDX1^{P33T/P33T}$ and $PDX1^{C18R/C18R}$ mutations in β-like cells, highlighting the regulatory function of this protein for insulin synthesis and secretion in human β-cells. This finding is supported by previous studies, reporting decreased binding activity of heterozygous P33T and C18R mutant PDX1 protein to human insulin promotor using electrophoretic mobility shift assay [15,16].

In summary, we report the impact of two common point mutations in the transactivation domain of PDX1 on human β-cell development and function and show that these mutations predispose to diabetes. Characterizing the impact of such mutations will expand our understanding of disease heterogeneity in the general population and might allow for diagnosing people at risk and predicting their susceptibility to diabetes or gestational diabetes [1]. Our previous study has revealed that the reduced level of Pdx1 promotes development of diabetes and gestational diabetes in male and female mice, respectively [56]. Here, we suggest a similar function of PDX1 in humans and propose that developmental and compensatory β-cell formation and expansion depends on a fully functional PDX1 TF.

AUTHOR CONTRIBUTION

X.W. performed and analyzed experiments. M.S. performed ChIP-seq experiments and computational analyses. A.B. helped to establish the FACS protocol. J.B. and J.S. helped to generate mutant lines. T.M. performed karyotyping. H.S. and H.-U.H. provided cells for iPSC generation. F.M.C. and G.S. provided infrastructure for ChIP-seq experiments and contributed to ChIP-seq analysis. M.I. and J.B. performed microarray and initial analysis of microarray data. C.V.E.W. provided the goat anti PDX1 antibody, used for ChIP experiments. A, I.B. and H.S. reviewed and edited the manuscript. X.W., M.S. and M.B. wrote the manuscript. H.L. wrote the manuscript and conceived the work. H.L. is the guarantor of this work.

ACKNOWLEDGEMENTS

CONFLICT OF INTEREST

The authors declare no conflicts of interest.

APPENDIX A. SUPPLEMENTARY DATA

Supplementary data to this article can be found online at https://doi.org/10.1016/j.molmet.2019.03.006.

REFERENCES

[1] Ahlqvist, E., Storm, P., Käräjämäki, A., Martinell, M., Dorkhan, M., Carlsson, A., et al., 2018. Novel subgroups of adult-onset diabetes and their association with outcomes: a data-driven cluster analysis of six variables. The Lancet Diabetes and Endocrinology 6(5):361—369. https://doi.org/10.1016/S2213-8587(18)30051-2.

[2] Diagnosis and classification of diabetes mellitus. Diabetes Care 37(Supplement_1), 2014:S81—S90. https://doi.org/10.2337/dc14-S081.

[3] Hattersley, A.T., Patel, K.A., 2017. Precision diabetes: learning from monogenic diabetes. Diabetologia, 769—777. https://doi.org/10.1007/s00125-017-4226-2.

[4] Staffers, D.A., Ferrer, J., Clarke, W.L., Habener, J.F., 1997. Early-onset type-II diabetes mellitus (MODY4) linked to IPF1. Nature Genetics 17(2):138—139. https://doi.org/10.1038/ng1097-138.

[5] Heuvel-Borsboom, H., de Valk, H.W., Losekoot, M., Westerink, J., 2016. Maturity onset diabetes of the young: seek and you will find. The Netherlands Journal of Medicine, 193—200.

[6] Ahlgren, U., Jonsson, J., Edlund, H., 1996. The morphogenesis of the pancreatic mesenchyme is uncoupled from that of the pancreatic epithelium in IPF1/PDX1-deficient mice. Development (Cambridge, England) 122(5):1409—1416. https://doi.org/10.1016/0092-8674(88)90391-1.

[7] Guz, Y., Montminy, M.R., Stein, R., Leonard, J., Gamer, L.W., Wright, C.V., et al., 1995. Expression of murine STF-1, a putative insulin gene transcription factor, in beta cells of pancreas, duodenal epithelium and pancreatic exocrine and endocrine progenitors during ontogeny. Development (Cambridge, England) 121(1):11—18.

[8] Offield, M.F., Jetton, T.L., Labosky, P.A., Ray, M., Stein, R.W., Magnuson, M.A., et al., 1996. PDX-1 is required for pancreatic outgrowth and differentiation of the rostral duodenum. Development (Cambridge, England) 122(3):983—995. https://doi.org/10.1016/0076-6879(93)25031-v.

[9] Ahlgren, U., Jonsson, J., Jonsson, L., Simu, K., Edlund, H., 1998. beta-cell-specific inactivation of the mouse Ipf1/Pdx1 gene results in loss of the beta-cell phenotype and maturity onset diabetes. Genes & Development 12(12): 1763—1768. https://doi.org/10.1101/gad.12.12.1763.

[10] Jonsson, J., Carlsson, L., Edlund, T., Edlund, H., 1994. Insulin-promoter-factor 1 is required for pancreas development in mice. Nature, 606—609. https://doi.org/10.1038/371606a0.

[11] Brissova, M., Shiota, M., Nicholson, W.E., Gannon, M., Knobel, S.M., Piston, D.W., et al., 2002. Reduction in pancreatic transcription factor PDX-1 impairs glucose-stimulated insulin secretion. Journal of Biological Chemistry 277(13):11225—11232. https://doi.org/10.1074/jbc.M111272200.

[12] Johnson, J.D., Ahmed, N.T., Luciani, D.S., Han, Z., Tran, H., Fujita, J., et al., 2003. Increased islet apoptosis in Pdx1+/- mice. Journal of Clinical Investigation 111(8):1147—1160. https://doi.org/10.1172/JCI200316537.

[13] Holland, A.M., Góñez, L.J., Naselli, G., MacDonald, R.J., Harrison, L.C., 2005. Conditional expression demonstrates the role of the homeodomain transcription factor Pdx1 in maintenance and regeneration of beta-cells in the adult pancreas. Diabetes 54(9):2586—2595. https://doi.org/10.2337/diabetes.54.9.2586.

[14] Stoffers, D.A., Stanojevic, V., Habener, J.F., 1998. Insulin promoter factor-1 gene mutation linked to early-onset type 2 diabetes mellitus directs expression of a dominant negative isoprotein. Journal of Clinical Investigation 102(1): 232–241. https://doi.org/10.1172/JCl2242.

[15] Gragnoli, C., Stanojevic, V., Gorini, A., Von Preussenthal, G.M., Thomas, M.K., Habener, J.F., 2005. IPF-1/MODY4 gene missense mutation in an Italian family with type 2 and gestational diabetes. Metabolism 54(8):983–988. https://doi.org/10.1016/j.metabol.2005.01.037.

[16] Macfarlane, W.M., Macfarlane, W.M., Frayling, T.M., Frayling, T.M., Ellard, S., Ellard, S., et al., 1999. Missense mutations in the insulin promoter factor-1 gene predispose to type 2 diabetes. Journal of Clinical Investigation 104. https://doi.org/10.1172/jci7449. R33-NaN-39.

[17] Fuchsberger, C., Flannick, J., Teslovich, T.M., Mahajan, A., Agarwala, V., Gaulton, K.J., et al., 2016. The genetic architecture of type 2 diabetes. Nature 536(7614):41–47. https://doi.org/10.1038/nature18642.

[18] Zhu, Z., Li, Q.V., Lee, K., Rosen, B.P., González, F., Soh, C.L., et al., 2016. Genome editing of lineage determinants in human pluripotent stem cells reveals mechanisms of pancreatic development and diabetes. Cell Stem Cell 18(6):755–768. https://doi.org/10.1016/j.stem.2016.03.015.

[19] Teo, A.K.K., Lau, H.H., Valdez, I.A., Dirice, E., Tjora, E., Raeder, H., et al., 2016. Early developmental perturbations in a human stem cell model of MODY5/HNF1B pancreatic hypoplasia. Stem Cell Reports 6(3):357–367. https://doi.org/10.1016/j.stemcr.2016.01.007.

[20] Shi, Z.D., Lee, K., Yang, D., Amin, S., Verma, N., Li, Q.V., et al., 2017. Genome editing in hPSCs reveals GATA6 haploinsufficiency and a genetic interaction with GATA4 in human pancreatic development. Cell Stem Cell 20(5):675–688. https://doi.org/10.1016/j.stem.2017.01.001 e6.

[21] Takahashi, K., Tanabe, K., Ohnuki, M., Narita, M., Ichisaka, T., Tomoda, K., et al., 2007. Induction of pluripotent stem cells from adult human fibroblasts by defined factors. Cell 107(5):861–872. https://doi.org/10.1016/j.cell.2007.11.019.

[22] Li, W., Wang, X., Fan, W., Zhao, P., Chan, Y.C., Chen, S., et al., 2012. Modeling abnormal early development with induced pluripotent stem cells from aneuploid syndromes. Human Molecular Genetics 21(1):32–45. https://doi.org/10.1093/hmg/ddr435.

[23] Millman, J.R., Xie, C., Van Dervort, A., Gürtler, M., Pagliuca, F.W., Melton, D.A., 2016. Generation of stem cell-derived β-cells from patients with type 1 diabetes. Nature Communications 7. https://doi.org/10.1038/ncomms11463.

[24] Shang, L., Hua, H., Foo, K., Martinez, H., Watanabe, K., Zimmer, M., et al., 2014. β-cell dysfunction due to increased ER stress in a stem cell model of wolfram syndrome. Diabetes 63(3):923–933. https://doi.org/10.2337/db13-0717.

[25] Zeng, H., Guo, M., Zhou, T., Tan, L., Chong, C.N., Zhang, T., et al., 2016. An isogenic human ESC platform for functional evaluation of genome-wide-association-study-identified diabetes genes and drug discovery. Cell Stem Cell 19(3):326–340. https://doi.org/10.1016/j.stem.2016.07.002.

[26] Wang, X., Sterr, M., Burtscher, I., Chen, S., Hieronimus, A., Machicao, F., et al., 2018. Genome-wide analysis of PDX1 target genes in human pancreatic progenitors. Molecular Metabolism 9:57–68. https://doi.org/10.1016/j.molmet.2018.01.011.

[27] Yumlu, S., Stumm, J., Bashir, S., Dreyer, A.-K., Lisowski, P., Danner, E., et al., 2017. Gene editing and clonal isolation of human induced pluripotent stem cells using CRISPR/Cas9. Methods 121–122:29–44. https://doi.org/10.1016/j.ymeth.2017.05.009.

[28] Heinz, S., Benner, C., Spann, N., Bertolino, E., Lin, Y.C., Laslo, P., et al., 2010. Simple combinations of lineage-determining transcription factors prime cis-regulatory elements required for macrophage and B cell identities. Molecular Cell 38(4):576–589. https://doi.org/10.1016/j.molcel.2010.05.004.

[29] Denny, S.K., Yang, D., Chuang, C.H., Brady, J.J., Lim, J.S.S., Grüner, B.M., et al., 2016. Nfib promotes metastasis through a widespread increase in chromatin accessibility. Cell 166(2):328–342. https://doi.org/10.1016/j.cell.2016.05.052.

[30] Love, M.I., Huber, W., Anders, S., 2014. Moderated estimation of fold change and dispersion for RNA-seq data with DESeq2. Genome Biology 15(12). https://doi.org/10.1186/s13059-014-0550-8.

[31] Ignatiadis, N., Klaus, B., Zaugg, J.B., Huber, W., 2016. Data-driven hypothesis weighting increases detection power in genome-scale multiple testing. Nature Methods 13(7):577–580. https://doi.org/10.1038/nmeth.3885.

[32] Zhu, A., Ibrahim, J.G., Love, M.I., 2018. Heavy-tailed prior distributions for sequence count data: removing the noise and preserving large differences. Bioinformatics. https://doi.org/10.1093/bioinformatics/bty895.

[33] Stefan, N., Machicao, F., Staiger, H., Machann, J., Schick, F., Tschritter, O., et al., 2005. Polymorphisms in the gene encoding adiponectin receptor 1 are associated with insulin resistance and high liver fat. Diabetologia 48(11): 2282–2291. https://doi.org/10.1007/s00125-005-1948-3.

[34] Wang, X., Chen, S., Burtscher, I., Sterr, M., Hieronimus, A., Machicao, F., et al., 2016. Generation of a human induced pluripotent stem cell (iPSC) line from a patient carrying a P33T mutation in the PDX1 gene. Stem Cell Research 17(2):273–276. https://doi.org/10.1016/j.scr.2016.08.004.

[35] Wang, X., Chen, S., Burtscher, I., Sterr, M., Hieronimus, A., Machicao, F., et al., 2016. Generation of a human induced pluripotent stem cell (iPSC) line from a patient with family history of diabetes carrying a C18R mutation in the PDX1 gene. Stem Cell Research 17(2):292–295. https://doi.org/10.1016/j.scr.2016.08.005.

[36] Rezania, A., Bruin, J.E., Arora, P., Rubin, A., Batushansky, I., Asadi, A., et al., 2014. Reversal of diabetes with insulin-producing cells derived in vitro from human pluripotent stem cells. Nature Biotechnology 32(11):1121–1133. https://doi.org/10.1038/nbt.3033.

[37] Smid, J.K., Faulkes, S., Rudnicki, M.A., 2015. Periostin induces pancreatic regeneration. Endocrinology 156(3):824–836. https://doi.org/10.1210/en.2014-1637.

[38] Bakhti, M., Böttcher, A., Lickert, H., 2018. Modelling the endocrine pancreas in health and disease. Nature Reviews Endocrinology. https://doi.org/10.1038/s41574-018-0132-z.

[39] Russ, H. a., Parent, A.V., Ringler, J.J., Hennings, T.G., Nair, G.G., Shveygert, M., et al., 2015. Controlled induction of human pancreatic progenitors produces functional beta-like cells in vitro. The EMBO Journal 34(13): e201591058. https://doi.org/10.15252/embj.201591058.

[40] Pagliuca, F.W., Millman, J.R., Gürtler, M., Segel, M., Van Dervort, A., Ryu, J.H., et al., 2014. Generation of functional human pancreatic β cells in vitro. Cell 159(2):428–439. https://doi.org/10.1016/j.cell.2014.09.040.

[41] Hattersley, A.T., Ashcroft, F.M., 2005. Activating mutations in Kir6.2 and neonatal diabetes: new clinical syndromes, new scientific insights, and new therapy. Diabetes, 2503–2513. https://doi.org/10.2337/diabetes.54.9.2503.

[42] Marshak, S., Benshushan, E., Shoshkes, M., Havin, L., Cerasi, E., Melloul, D., 2000. Functional conservation of regulatory elements in the pdx-1 gene: PDX-1 and hepatocyte nuclear factor 3beta transcription factors mediate beta-cell-specific expression. Molecular and Cellular Biology 20(20):7583–7590. https://doi.org/10.1128/MCB.20.20.7583-7590.2000.

[43] Gerrish, K., Cissell, M.A., Stein, R., 2001. The role of hepatic nuclear factor 1α and PDX-1 in transcriptional regulation of the pdx-1 gene. Journal of Biological Chemistry 276(51):47775–47784. https://doi.org/10.1074/jbc.M109244200.

[44] Gerrish, K., Van Velkinburgh, J.C., Stein, R., 2004. Conserved transcriptional regulatory domains of the pdx-1 gene. Molecular Endocrinology (Baltimore, Md.) 18(3):533–548. https://doi.org/10.1210/me.2003-0371.

[45] Akerman, I., Tu, Z., Beucher, A., Rolando, D.M.Y., Sauty-Colace, C., Benazra, M., et al., 2017. Human pancreatic β cell lncRNAs control cell-specific regulatory networks. Cell Metabolism 25(2):400–411. https://doi.org/10.1016/j.cmet.2016.11.016.

[46] Mamidi, A., Prawiro, C., Seymour, P.A., de Lichtenberg, K.H., Jackson, A., Serup, P., et al., 2018. Mechanosignalling via integrins directs fate decisions

of pancreatic progenitors. Nature 564(7734):114—118. https://doi.org/10.1038/s41586-018-0762-2.

[47] You, L., Wang, N., Yin, D., Wang, L., Jin, F., Zhu, Y., et al., 2016. Down-regulation of long noncoding RNA Meg3 affects insulin synthesis and secretion in mouse pancreatic beta cells. Journal of Cellular Physiology 231(4):852—862. https://doi.org/10.1002/jcp.25175.

[48] Kameswaran, V., Bramswig, N.C., McKenna, L.B., Penn, M., Schug, J., Hand, N.J., et al., 2014. Epigenetic regulation of the DLK1-MEG3 MicroRNA cluster in human type 2 diabetic islets. Cell Metabolism 19(1):135—145. https://doi.org/10.1016/j.cmet.2013.11.016.

[49] Vrang, N., Meyre, D., Froguel, P., Jelsing, J., Tang-Christensen, M., Vatin, V., et al., 2010. The imprinted gene neuronatin is regulated by metabolic status and associated with obesity. Obesity 18(7):1289—1296. https://doi.org/10.1038/oby.2009.361.

[50] Millership, S.J., Da Silva Xavier, G., Choudhury, A.I., Bertazzo, S., Chabosseau, P., Pedroni, S.M.A., et al., 2018. Neuronatin regulates pancreatic β cell insulin content and secretion. Journal of Clinical Investigation 128(8):3369—3381. https://doi.org/10.1172/JCI120115.

[51] Grarup, N., Moltke, I., Andersen, M.K., Bjerregaard, P., Larsen, C.V.L., Dahl-Petersen, I.K., et al., 2018. Identification of novel high-impact recessively inherited type 2 diabetes risk variants in the Greenlandic population. Diabetologia 61(9):2005—2015. https://doi.org/10.1007/s00125-018-4659-2.

[52] Locke, J.M., Hysenaj, G., Wood, G., Weedon, M.N., Harries, L.W., 2015 Apr. Targeted allelic expression profiling in human islets identifies cis-regulatory effects for multiple variants identified by type 2 diabetes genome-wide association studies. Diabetes 64(4):1484—1491. https://doi.org/10.2337/db14-0957.

[53] Quiroga, A.D., Li, L., Trötzmüller, M., Nelson, R., Proctor, S.D., Köfeler, H., et al., 2012. Deficiency of carboxylesterase 1/esterase-x results in obesity, hepatic steatosis, and hyperlipidemia. Hepatology (Baltimore, Md.) 56(6):2188—2198. https://doi.org/10.1002/hep.25961.

[54] Pan, F.C., Brissova, M., Powers, A.C., Pfaff, S., Wright, C.V.E., 2015. Inactivating the permanent neonatal diabetes gene Mnx1 switches insulin-producing β-cells to a δ-like fate and reveals a facultative proliferative capacity in aged β-cells. Development 142(21):3637—3648. https://doi.org/10.1242/dev.126011.

[55] Flanagan, S.E., De Franco, E., Lango Allen, H., Zerah, M., Abdul-Rasoul, M.M., Edge, J.A., et al., 2014. Analysis of transcription factors key for mouse pancreatic development establishes NKX2-2 and MNX1 mutations as causes of neonatal diabetes in man. Cell Metabolism 19(1):146—154. https://doi.org/10.1016/j.cmet.2013.11.021.

[56] Bastidas-Ponce, A., Roscioni, S.S., Burtscher, I., Bader, E., Sterr, M., Bakhti, M., et al., 2017. Foxa2 and Pdx1 cooperatively regulate postnatal maturation of pancreatic β-cells. Molecular Metabolism 6(6):524—534. https://doi.org/10.1016/j.molmet.2017.03.007.

[57] Kleinert, M., Clemmensen, C., Hofmann, S.M., Moore, M.C., Renner, S., Woods, S.C., et al., 2018. Animal models of obesity and diabetes mellitus. Nature Reviews Endocrinology, 140—162. https://doi.org/10.1038/nrendo.2017.161.